The protocol for differentiation induction culture is summarized in Figure 1. Human iPS/ES cells were culture on matrigel-coated dishes in RPMI1640 medium supplemented with 2 mM L-glutamine, 100 μM 2-mercaptoethanol, 20 U/mL penicillin 20 μg/mL streptomycin, and 0.29% recombinant human albumin (Mitsubishi Tanabe Pharma Corp., Osaka, Japan) in the presence of 100 ng/mL Activin A (PeproTech, Rocky Hill, NJ), and 25 ng/mL Wnt 3A (R&D Systems Inc., Minneapolis, MN) for 24 h, followed by another 24-h culture in the presence of Activin A alone in the presence of 0.2% KSR (Invitrogen). After 48 h from the beginning of differentiation culture, the cells were subjected to the next stage of culture and were cultured with mixtures of three cytokines, fibroblast growth factor-2 (FGF-2; PeproTech; 10 ng/mL), bone morphogenic protein-4 (BMP-4; Wako Pure Chemical Industry; 20 ng/mL) and Sonic hedgehog (Shh; R&D; 200 ng/mL) in the presence of 2% KSR for 5 days. Then, the cells were culture with hepatocyte growth factor (HGF; R&D; 20 ng/mL), FGF-2 (10 ng/mL), and BMP-4 (20 ng/mL) for another 5 days in similar medium. Finally, cells were culture in the presence of oncostatin M (R&D; 10 ng/mL) and dexamethasone (0.1 μM) for final hepatic maturation for 6 to 16 days.

Reverse transcription-polymerase chain reaction (RT-PCR)

Total RNA was extracted from the cultured cells using TRIzol Reagent (Life Technologies co., Carlsbad, CA). For reverse transcription reactions, 1 μg RNA was reverse-transcribed using Superscript™ III First-Strand Synthesis System for RT-PCR (Invitrogen). A total of 0.5 μL of cDNA was used for PCR analysis. PCR amplification of different genes was performed using rTaq (Takara, Tokyo, Japan), with a program comprising 94°C for 5 min, 35 cycles of 94°C for 30 sec, 50–60°C for 30 sec, 72°C for 30 sec, and a final extension at 72°C for 10 min. The sequence of the primers used are as follows: α-fetoprotein (AFP); a forward primer 5′-TTTTG GGACCCGAACTTTCC-3′ and a reverse primer 5′-CTCCT GGTATCCTTTAGCAACTCT-3′, albumin (ALB); a forward primer 5′-GGTGTTGATTGCCTTTGCTC-3′ and a reverse primer 5′-CCCTTCATCCCGAAGTTCAT-3′, α1-antitrypsin (AAT); a forward primer 5′-ACATTTACCCAAACTGTCCA TT-3′ and a reverse primer 5′-GCTTCAGTCCCTTTCTC GTC-3′, cytochrome P450 3A4 (CYP3A4); a forward primer 5′-ATGAAAGAAAGTCGCCTCG-3′ and a reverse primer 5′-TGGTGCCTTATTGGGTAA-3′, hepatocyte nuclear factor 4α (HNF-4α); a forward primer 5′-CCACGGGCAAACA CTACGG-3′ and a reverse primer 5′-GGCAGGCTGCTGT CCTCAT-3′, tyrosine aminotransferase (TAT); a forward primer 5′-CCCCTGTGGGTCAGTGTT-3′ and a reverse primer 5′-GTGCGACATAGGATGCTTTT-3′, tryptophan 2, 3-dioxygenase (TDO2); a forward primer 5′-TACAGAGCAC TTCAGGGAG-3′ and a reverse primer 5′-CTTCGGTATCC AGTGTCG-3′, glyceraldehyde 3 phosphate dehydrogenase (GADPH); a forward primer 5′-GAAGGTGAAGGTCGGA GTC-3′ and a reverse primer 5′- GAAGATGGTGATGGG ATTTC-3′.

Quantitative RT-PCR

Total RNA was isolated by using TRIzol reagent and cDNA was synthesized in 20 μL of reaction volume containing 1 μg of total RNA and Superscript™ III First-Strand Synthesis System for RT-PCR (Invitrogen) in accordance with the manufacturer's instructions. Duplex real-time PCR (target gene and glyceraldehyde 3 phosphate dehydrogenase (GAPDH) as a reference gene) in 96-well optical plates was performed using TaqMan® technology and analyzed using an ABI PRISM® PE7900 HT sequence Detection System (Perkin-Elmer Applied Biosystems, Lincoln, CA). PCR mix per well (25 μL) consisted of commercially available, premixed GAPDH TaqMan® primers/probe, TaqMan® Gene Expression Assays, inventoried primers/probe for the target gene, 0.5 μL cDNA and QuantiTect® Multiplex PCR Master Mix (Qiagen, Valencia, CA). PCR conditions were as follows: 50°C for 2 min, 95°C for 10 min, followed by 40 cycles of 95°C for 15 sec, and 60°C for 1 min. The expression level of each gene was normalized to RNA content for each sample by using GAPDH as an internal control.

Western blotting

Western blotting was performed using rabbit polyclonal antihuman AFP (Epitomics Inc., Burlingame, CA), rabbit polyclonal antihuman ALB (DakoCytomation, Glostrup, Denmark), rabbit polyclonal antihuman AAT (Lifespan Bioscience Inc., Seattle, WA), and rabbit polyclonal anti-human CYP 3A4 antibodies (Abcam, Cambridge, UK). The second antibody reaction was performed using a horseradish peroxidase-conjugated antirabbit or antimouse IgG (Cell Signaling Technology, Inc., Beverly, MA). The final detection procedure was performed using ECL Western blotting detection reagents (GE Healthcare UK Ltd., Buckinghamshire, UK).

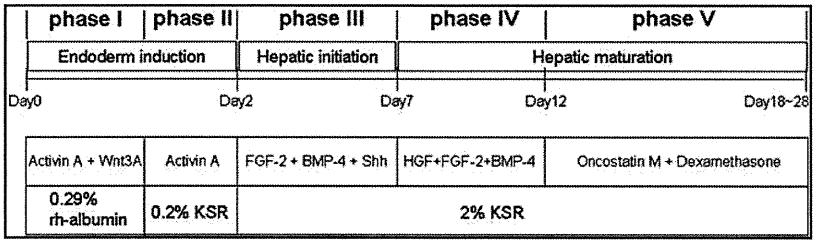

FIG. 1. Schematic presentation of feeder-free and serum-free production of functional hepatocytes from human iPS and ES cells. Undifferentiated human iPS and ES cells were induced to differentiate into hepatocytes using a five phase culture system that mimics developmental process of liver *in vivo*. Abbreviations: FGF-2: fibroblast growth factor 2, BMP-4: bone morphogenic protein 4, Shh: Sonic hedgehog, HGF: hepatocyte growth factor, KSR: Knockout™ Serum Replacement, rh-albumin: recombinant human albumin.

Immunostaining

The cells were fixed with acetone/methanol solution (1:3), permeabilized with 0.1% Triton X-100 in phosphate-buffered saline and blocked with BlockAce (DS Pharma Biomedical). The immunostaining procedure was performed with primary antibody reactions using a rabbit polyclonal antihuman AFP antibody (Epitomics), rabbit polyclonal antihuman AAT antibody (Lifespan Bioscience), rabbit polyclonal antihuman CYP3A4 (Abcam), mouse monoclonal antihuman epithelial cell adhesion molecule (EpCAM) antibody (Cell Signaling Technology), and a rabbit polyclonal antihuman ALB antibody (DakoCytomation), followed by secondary antibody reactions using Alexa Fluor® 488 chicken antimouse IgG (H+L), Alexa Fluor® 568 goat anti-rabbit IgG (H+L) or Alexa Fluor® 594 chicken antigoat IgG (H+L) (Invitrogen) antibodies.

Periodic Acid Schiff (PAS) assay for glycogen storage

Glycogen storage was measured by PAS staining a using a PAS staining kit (Muto Pure Chemicals, Tokyo, Japan) in accordance with the manufacturer's instructions.

Cellular uptake and release of Indocyanine Green (ICG)

ICG (Sigma-Aldrich, St. Louis, MO) was dissolved in DMSO to make a stock at 5 mg/mL and then freshly diluted in culture medium to 1 mg/mL. After incubation of cells with ICG (Sigma-Aldrich) for 30 min at 37°C, the medium with ICG was discarded and washed three times with phosphate-buffered saline, and the cellular uptake of ICG was examined by microscopy. Cells were then returned to the culture medium and incubated for 6 h for the release of cellular ICG stain.

Cytochrome P450 activity assay

CYP3A4 activity was evaluated using a p450-GloTM CYP3A4 Assay kit (Promega, Madison, WI). The cells were treated with or without dexamethasone (50 μM) for 16 h for induction and were then incubated with culture medium supplemented with 50 μM CYP3A4 substrates in accordance with the manufacturer's instructions. At 4 h after treatment, 50 μL of culture medium was removed and assayed in a luminometer. CYP450 activities were expressed as relative light units (RLU/mL).

Hepatocyte toxicity assay by D-galactosamine (D-GalN)

The cells were treated with 25 mM D-GalN for 24 h at 37°C, and then the supernatant was collected. Glutamic oxaloacetic transaminase (GOT), glutamic pyruvic transaminase (GPT), γ-glutamyl transpeptidase (γ-GTP), leucine aminopeptidase (LAP), and isozymes of lactate dehydrogenase (LDH) in the culture medium were measured sing a routine colorimetric laboratory method. In some experiments, cells were preincubated with 4 mM prostaglandin E1 (PGE1) for 4 h at 37°C before D-GalN was added.

Transmission electron microscopy

The samples were fixed using 2.5% glutaraldehyde in 0.1 M PBS (pH 7.4) for 2 h. After washing with PBS, samples were postfixed with 2% osmium tetraoxide for 1 h. Samples were dehydrated in a series of ascending ethanol concentrations and placed in propylene oxide prior to embedding in epoxy resin (Sakura Finetek Japan, Tokyo, Japan). After resin polymerization, sections of approximately 60~80 nm were cut using Ultracuts (Reichert Scientific Instruments Co., Buffalo, NY) and double stained with uranyl acetate and lead citrate. Electron micrographs were taken using a Hitachi H-7500 transmission electron microscope (Hitachi High-Technologies Corp., Tokyo, Japan).

Cell proliferation assay

We used a Cellomics® BrdU and Ki-67 cell proliferation kit (Thermo Fisher Scientific Inc., Waltham, MA) and the assay was performed in accordance with the manufacturer's instructions. The cells were labeled with 120 μM BrdU for 20 h and then permeabilized and incubated with mouse anti-BrdU and rabbit

FIG. 2. Molecular characterization of hepatocytes induced from human iPS and ES cells. (**A**) RT-PCR analysis of hepatocyte-specific marker genes (AFP: α-fetoprotein, ALB: Albumin, AAT: α1-antitrypsin, HNF-4α: hepatocyte nuclear factor 4α, TAT: tyrosine aminotransferase, CYP3A4: cytochrome P450 3A4, TDO2: tryptophan 2, 3-dioxygenase, GADPH: glyceraldehyde-3-phosphate dehydrogenase) in undifferentiated human iPS cells (253G1) and cells derived from human iPS cells (253G1) during differentiation inducting cultures. Each lane of the RT-PCR analysis indicated undifferentiated human iPS cells (253G1) cultured on MEF (U1), undifferentiated human iPS cells cultured on Matrigel (U2), induced cells on the first (1), second (2), seventh (7), and seventeenth (17) days of differentiation. (**B**) Quantitative RT-PCR analysis of three hepatocyte-specific marker genes (TDO2, CYP3A4, TAT) in undifferentiated human iPS cells (253G1) and cells derived from human iPS cells (253G1) during differentiation induction cultures. As a control (CTL), two human hepatic cell lines were used. These two cell lines were HepaRG cells (HepaRG) and HpG2 cells (HepG2). The sign " $\approx$ " on the top of the HepaRG signal for CYP3A4 indicates that the value was beyond the vertical scale of the graph and the relative value was 1.033. (**C**) Western blot analysis of hepatocyte-specific markers (AFP: α-fetoprotein, ALB: Albumin, AAT: α1-antitrypsin, CYP3A4: cytochrome P450 3A4) in undifferentiated (U) human iPS cells (253G1, #40, and SeV5 cells) and human ES cells (K1: KhES-1 cells) and induced cells on the 29th day of differentiation (H). As a control (CTL), two human hepatic cell lines were used. These two cell lines were HepaRG cells (HepaRG) and HpG2 cells (HepG2). (D) Immunostaining of hepatocyte-specific markers of cells induced from human iPS cells (#40) and human ES cells (K1: KhES-1 cells). Human iPS and ES cells were induced to differentiate for 29 days and were stained using an isotype control antibody (IgG), a rabbit polyclonal antihuman α-fetoprotein (AFP) antibody, a rabbit polyclonal antihuman albumin antibody (ALB), or a rabbit polyclonal antihuman α-1 antitrypsin (AAT) as indicated. A total 1 μg/mL DAPI was used to stain the cell nucleus. Scale bar=50 mm. (E) Immunostaining of hepatocyte-specific markers of HepaRG cells were performed using an isotype control antibody (IgG), a rabbit polyclonal antihuman α-fetoprotein (AFP) antibody, or a rabbit polyclonal anti-human α-1 antitrypsin (AAT) antibody as indicated. A total of 1 μg/mL DAPI was used to stain the cell nucleus. Scale bar=50 mm.

anti-Ki-67 antibodies for 60 min at 37°C. After washing, the cells were incubated with Alexa Fluor 488-conjugated goat anti-mouse IgG, Alexa Fluor 549-conjugated goat antirabbit IgG and DAPI, washed twice, and mounted on glass slides with ProLong® Gold antifade reagent (Invitrogen). The slides were subsequently inspected using a fluorescence microscope.

Experiments for passages and regrowth of induced hepatocytes

At the 28th day of differentiation, induced hepatocytes were collected from the original culture dishes using a StemPro® EZPassage™ Disposable Stem Cell Passaging Tool

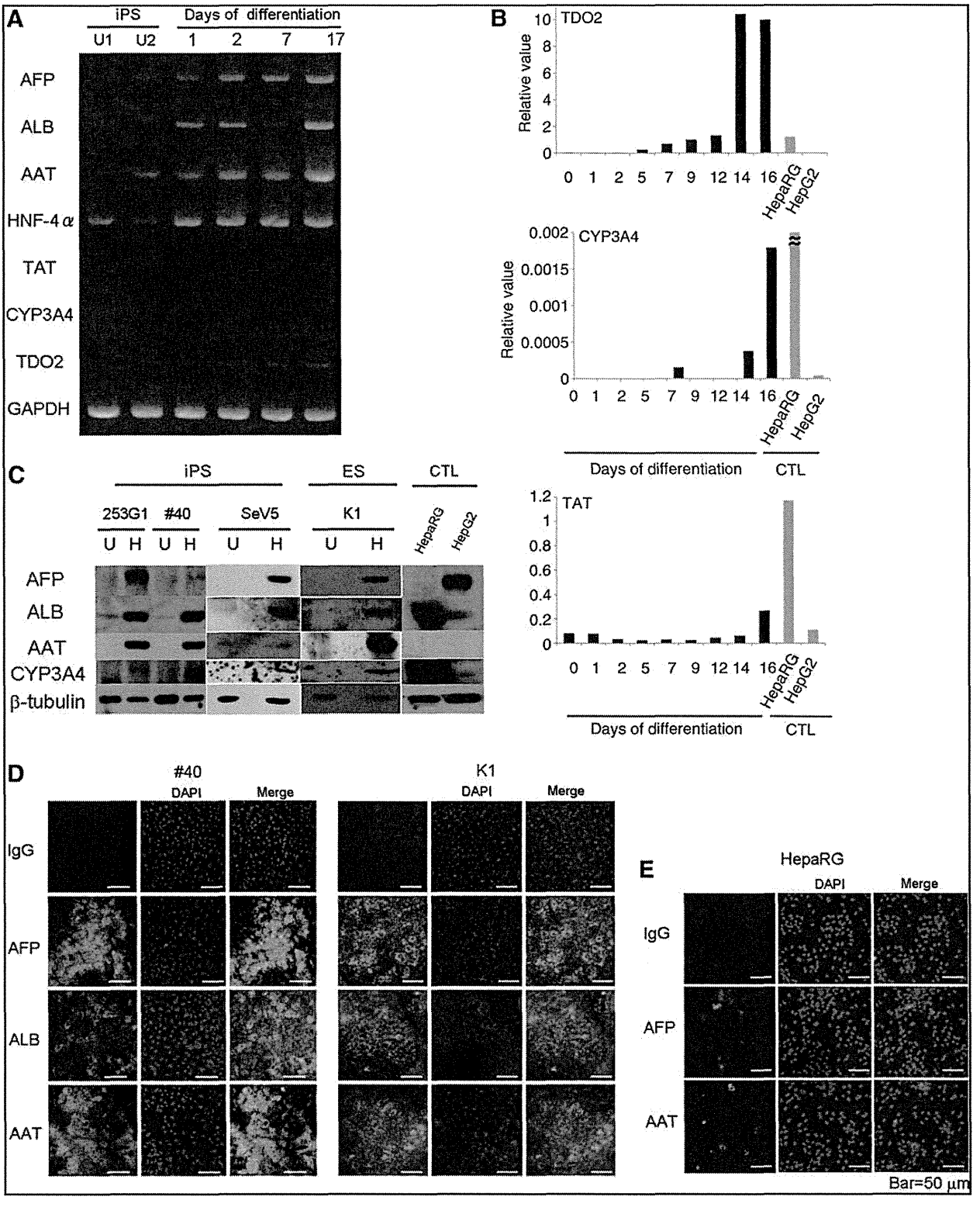

(Invitrogen) and were recultured in new 3.5 mmϕcollagen-coated dishes (ASAHI GLASS Co., Ltd., Tokyo, Japan).

Results

Feeder-free and serum-free culture methods for hepatocyte differentiation of human iPS and ES cells

After a process of trial and error, we found that the key to success in inducing endodermal differentiation of human ES/iPS cells resided in preparing the starting materials at appropriate densities, that is, to seed the undifferentiated human ES/iPS cells so that the clumps of cells were just contacting one another. By using these appropriately seeded cells, we successfully performed a three-stage (five-phase) differentiation protocol for the induction of functional hepatocytes from human iPS and ES cells (Fig. 1).

In the initial experiment, we performed differentiation induction of human iPS cells (253G1) established from adult human dermal fibroblasts using retrovirus vectors, because this cell line is one of the standard iPS cell lines in Japan and was established without using a protooncogene c-Myc. During differentiation induction, we analyzed time courses of expression of hepatocyte-specific genes (AFP, ALB, and hepatocyte-specific metabolic enzymes). As shown in Figure 2A, transcriptional expression of hepatocytes-specific markers such as AFP, ALB, AAT, tyrosine aminotransferase (TAT), CYP3A4, and tryptophan 2, 3-dioxygenease (TDO2) were observed during differentiation, although the expression levels of TAT, CYP3A4, and TDO2 were slightly weaker than the other markers. To evaluate more quantitatively, we then performed quantitative real time PCR studies of these three markers, TAT, CYP3A4, and TDO2 and compared them with those of human hepatocyte cell lines, HepaRG and HepG2. As shown in Figure 2B, cellular expression of these three markers was detected in a time-dependent manner and the level of their expression was quantitatively equivalent to or sometimes much better than the level of human hepatocyte cell lines.

We then confirmed the expression of hepatocyte markers at the protein level. In these experiments, we also used two other human iPS cell lines, one was #40 established from fetal fibroblasts using a retrovirus vector, and the other was SeV5 established from neonatal fibroblasts using Sendai virus vector, without integration of viral vector components and transgenes. As shown in Figure 2C, several hepatocyte markers, such as AFP, ALB, AAT, and CYP3A4, were induced in all three human iPS cells. The level of induction was similar to that of human hepatocyte cell lines. In particular, AAT, which was not detected in control human hepatocyte cell lines, was prominently induced in human iPS cells. These findings were further confirmed using human ES cells (KhES-1) (Fig. 2C). Protein expression of AFP, ALB, and AAT was also confirmed by immunostaining (Fig. 2D), and overall positivity for these three markers was approximately 30–60%. In contrast, protein expression of AFP and AAT in HepaRG cells as determined by immunostaining was weak and positivity was less than 20% (Fig. 2E).

Functional evaluation of hepatocytes induced from human iPS and ES cells

To clarify whether human hepatocytes induced from human pluripotent stem cells possessed the functional capacity of mature hepatocytes, we performed three standard assays, ICG-uptake capacity, glycogen storage capacity, and CYP450 activity. As shown in Figure 3A, hepatocytes differentiated from human iPS cells (253G1, #40, and SeV5) and human ES cells (KhES-1) all showed clear uptake of ICG, and this ICG was released after 6 h. The overall level of ICG uptake-positive cells was approximately 20–30%. HepaRG and HepG2 cells showed substantial capacity (20–30% for HepaRG cells and less than 5% for HepG2 cells). Thus, hepatocytes from human iPS and ES cells have sufficiently mature functions for hepatocytes compared with the levels in control hepatocytes.

Then, we evaluated cytoplasmic glycogen accumulation in undifferentiated human iPS and ES cells and hepatocytes induced from these pluripotent stem cells, and found that almost all (more than 80%) of hepatocytes induced from human iPS and ES cells were strongly positive for PAS staining, whereas undifferentiated human iPS and ES cells were not stained (Fig. 3B). On the other hand, HepaRG cells were almost 50–60% positive, and Hep G2 cells were negative.

It has been reported that CYP3A4 plays a central role in drug metabolism and detoxification in the liver among a subfamily of CYP450s (Liu et al., 2007), and we identified the expression of this critical enzyme during our differentiation culture at both mRNA (Fig. 1) and protein (Fig. 2) levels. We then determined the functional activity of CYP3A4 using hepatocytes differentiated from human iPS and ES cells. As shown in Figure 3C, hepatocytes induced from human iPS and ES cells showed high levels of CYP3A4 activity compared with those of undifferentiated human iPS and ES cells and human hepatic cell lines, HepaRG and HepG2 cells. In addition, high CYP3A4 activity in the differentiated cells was further potentiated by transient (16 h) pharmacological induction in hepatocytes induced from human iPS cells (#40) and human ES cells (KhES-1).

Hepatocyte toxicity assay using D-galactosamine

It is essential to establish an *in vitro* hepatocyte cytotoxic assay for the evaluation of liver toxicity of various substance and/or drugs. Therefore, we performed an *in vitro* cytotoxic assay with hepatocytes induced from human pluripotent stem cells using a traditional method with D-GalN (Bao and Liu, 2010; Kuhla et al., 2009; Siendones et al., 2005). GOT, GPT, γ-GTP, LAP, and LDH isozymes released from the cells were quantified as an indicator of hepatocyte-specific cytotoxicity.

As shown in Figure 4A, D-GalN significantly and potently induced the extracellular release of GOT, GPT, and/or LDH into the culture medium, and the pattern of LDH was hepatocyte-specific (LDH4/5 dominant) in hepatocytes induced from human iPS and ES cells. These cytotoxic effects of D-GalN were significantly inhibited by PGE1 (Fig. 4B) (Siendones et al., 2005). In contrast, D-GalN only minimally induced the extracellular release of these hepatocyte-specific enzymes in undifferentiated human iPS and ES cells and human umbilical vein endothelial cells (HUVECs). Extracellular release of GOT, GPT, and LDH5 into the medium was also observed in control hepatocytes, HepaRG and HepG2 cells. Interestingly and unexpectedly, γ-GTP and LAP, which are bile duct specific enzymes, were released from "hepatocytes" induced from human iPS and ES cells

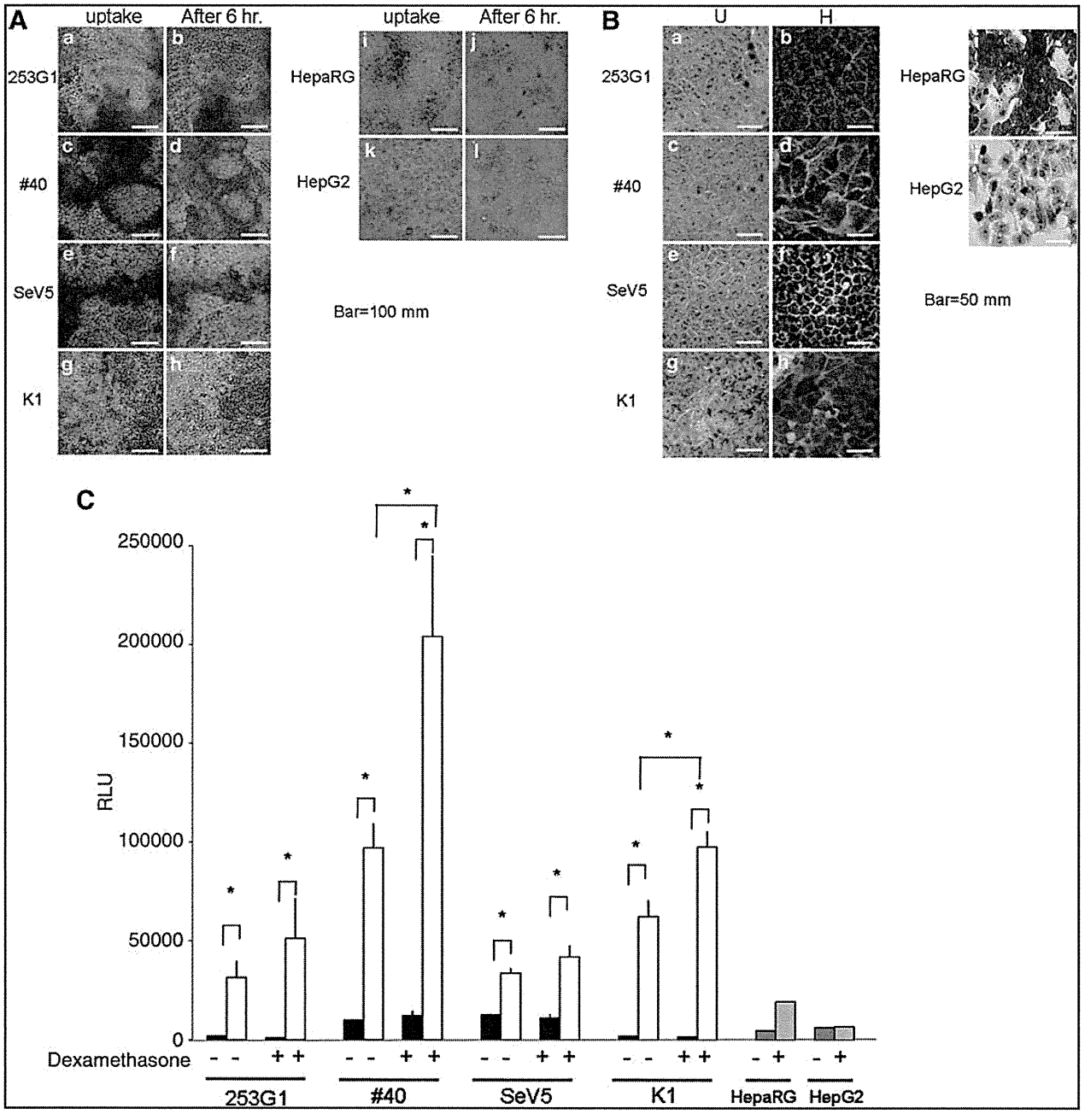

FIG. 3. Functional activity .of hepatocytes induced from human iPS and ES cells. (**A**) Indocyanine green (ICG) uptake and release. Hepatocytes induced from three human iPS cells (253G1, #40, and SeV5 cells) and ES cells (K1: KhES-1 cells) (on the 29th day of differentiation culture) and HepaRG cells (HepaRG) and HepG2 cells (Hep G2) were examined for their ability to take up ICG (left column, a, c, e, g, i, and k) and release it 6 h thereafter (right column, b, d, f, h, j, and l). Scale bar = 50 mm. (**B**) Glycogen storage ability as evaluated by Periodic Acid Schiff (PAS) staining were determined for hepatocytes induced from three human iPS cells (253G1, #40, and SeV5 cells) and ES cells (K1:KhES-1 cells) (on the 29th day of differentiation culture) and HepaRG cells (HepaRG) and HepG2 cells (Hep G2). Nuclei were counterstained with hematoxylin. Glycogen storage is indicated by pink or dark red-purple cytoplasms. Scale bar = 50 mm. (**C**) CYP3A4 activity and its induction by dexamethasone were determined using assay kit and expressed as relative light units (RLU) per milliliter of culture medium. Solid bar, open bar, and gray bar represent undifferentiated human ES/iPS cells, induced hepatocytes, and control human hepatic cell lines, respectively. Data for undifferentiated human ES/iPS cells and induced hepatocytes are presented as mean ± SD from triplicate experiments ($*p < 0.05$), and data of control human hepatic cell lines are the means of single experiment.

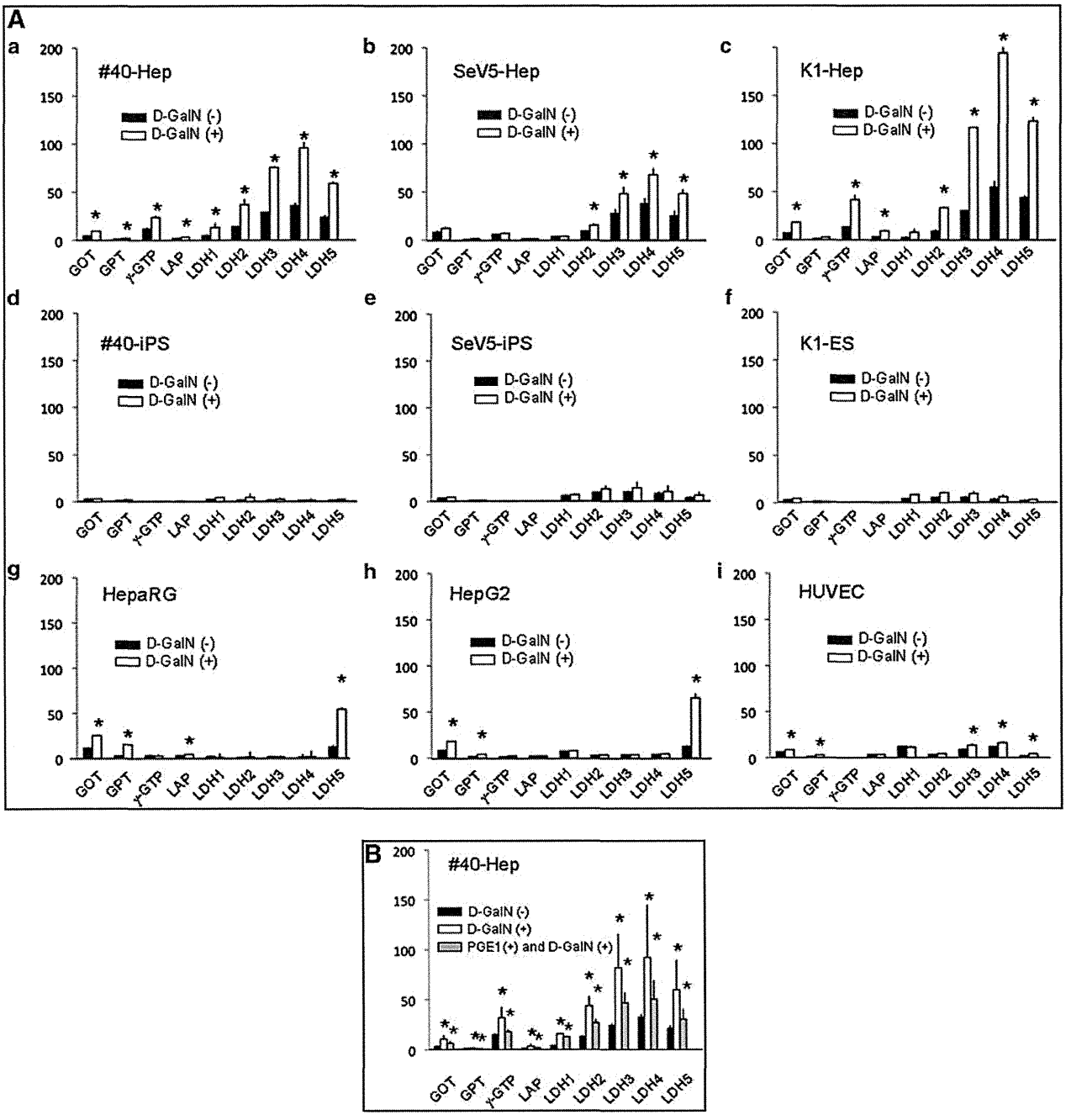

FIG. 4. D-galactosamine cytotoxic assay. (**A**) Cells were incubated with 25 mM D-galactosamine (D-GalN) for 24 h at 37°C. Liver-specific enzymes (GOT, GTP, γ-GTP, LAP, isozymes of LDH) released from the cells into the culture medium were measured using a routine colorimetric laboratory method and expressed as mean ± SD of triplicate assays. Hepatocytes induced from two human iPS cells (#40-Hep, SeV5-Hep) and ES cells (K1-Hep) (on the 29th day of differentiation culture), undifferentiated iPS/ES cells (#40-iPS, SeV5-iPS, K1-ES) and HepaRG cells (HepaRG), HepG2 cells (HepG2) and human umbilical vein endothelial cells (HUVEC) were used in this assay. $^*p < 0.05$. (**B**) The cells were preincubated with 2 mM prostaglandin E1 (PGE1) for 2 h at 37°C, and were then incubated with 25 mM D-galactosamine (D-GalN) for 24 h at 37°C. Liver-specific enzymes (GOT, GTP, γ-GTP, LAP, isozymes of LDH) released from the cells into the culture medium were measured by a colorimetric routine laboratory method and expressed as mean ± SD of triplicate assays. Hepatocyte-like cells induced from human iPS cells (#40-Hep) at the 29th days of differentiation were used in this assay. $^*p < 0.05$.

but not undifferentiated human iPS and ES cells, HUVEC, and control hepatocytes (HepaRG and HepG2 cells). These findings suggest that "hepatocytes" induced from human iPS and ES cells include not only hepatocytes themselves but also bile duct-related cells such as cholangiocytes. Thus, our culture system could be useful for cytotoxicity assays for both hepatocytes and cholangiocytes.

Electron microscopic study of hepatocytes and cholangiocytes in our culture system

To confirm that the "hepatocytes" induced from human pluripotent stem cells were really hepatocytes and explore possible coexistence of bile ducts, bile canaliculi, and cholangiocytes in the culture system, we performed detailed morphological examinations of differentiated cells using an electron microscope.

As shown in Figure 5A, hepatocytes induced from human ES cells were equipped with microvilli of intermediate length (shorter than the microvilli in the intestine) on their open space-side ["space of Disse" (perisinusoidal space) in the liver] and adjacent cells were connected via structures such as tight junctions and desmosomes. Between the cells, there was a microduct-like structure with microvilli on the lumen side, which was considered to be bile canaliculus, and this microduct-like structure was also joined by cell–cell connecting structures (tight junctions and desmosomes). Abundant glycogen α-particles were observed in the cytoplasm, and these glycogen α-particles showed a hepatocyte-specific "rosette formation." We also observed "peroxisomes," cytoplasmic structures highly specific for hepatocytes. Similar microscopic findings were observed in hepatocyte-like cells induced from human iPS cells (Fig. 5B). In addition, typical structures specific for bile ducts were also observed, that is, bile duct epithelial cells with short microvilli on the lumen side and the basement membrane on the other side were observed (Fig. 5C).

Thus, there existed at least three cell types and structures, hepatocytes, bile canaliculi (intrahepatic microbile duct) and bile duct epithelial cells, and all of these microstructures are extremely specific for the liver (Ghadially, 1997).

Possible existence of bipotential hepatoblasts with proliferating capacity

Data presented in Figures 4 and 5 together clearly indicate the presence of both hepatocytes and cholangiocytes in the present culture system. It is has been proposed that both hepatocytes and cholangiocytes are derived from their common progenitor cells called hepatoblasts (Zhao and Duncan, 2005). We then explored the presence of immature progenitors with proliferating potential.

Figure 6A shows cell morphologies observed using an inverted microscope. Two forms of cell structures and/or areas were observed: one was a bulging cell clump area, and the other was a flattened monolayer area containing binuclear cells. These two areas were analyzed using immunostaining for AFP and EpCAM, both of which are hepatoblasts markers (Schmelzer et al., 2006). As shown in Figure 6B, the bulging areas were stained positively for both markers, whereas the flattened areas were not. These findings suggested that the present culture system mainly contained two populations: one in the bulging area with proliferating immature cells with hepatoblast markers, and the other in the flattened mature hepatocyte area. The former area was also positive for proliferation marker Ki-67 (Fig. 6C), and the latter areas were also positive for ALB, a mature hepatocyte marker (Fig. 6D). In addition, we confirmed these findings in a single microscopic field; namely, the bulging area was positive for BrdU, a proliferation marker, and the flattened area was positive for AAT, a mature hepatocyte marker (Fig. 6E). Thus, the bulging area with frequent cell nuclei (stained by DAPI) was positive for proliferation markers (Ki-67 and BrdU) and hepatoblast markers (AFP and EpCAM), whereas the flattened area had fewer cell nuclei (stained by DAPI) and was negative or weakly positive for proliferating markers and positive for mature hepatocyte markers (ALB and AAT).

To further confirm the proliferative potential of "hepatocytes" from human pluripotent stem cells, we performed passages of differentiated cells into new culture dishes. Induced hepatocytes were collected from the original culture dish and recultured in new dishes. After attaching to the new dish, cells began to proliferate again (Fig. 6F, upper panel). On the second day of reculture, colonies of small-sized cells (10–20 μm vs. 20–60 μm; cells of flattened areas in Fig. 6A) appeared and expanded during reculture for up to 9 days (Fig. 6F, upper panel). These small-sized cells were positive for AFP and AAT (Fig. 6F, lower panel).

Thus our differentiation culture included not only mature hepatocytes but also their precursors with proliferation potential and began to proliferate again even after transfer to new culture dishes along with positive results for hepatocyte markers.

Discussion

In the present study, we established a feeder-free and serum-free induction system for human mature, functional hepatocytes from human pluripotent stem cells, iPS, and ES cells. We found that an initial high density culture, so that each colony of undifferentiated human ES/iPS cells was contacting other colonies, was essential in order to start stable and reproducible differentiation. In addition, we used a high concentration of Activin A and added Wint 3A to induce effective initial endoderm differentiation (Hay et al., 2008a). We also added Shh during second-step differentiation because Hedgehog has been reported to play important roles during liver development in embryos (Hirose et al., 2009) and liver regeneration after hepatectomy (Ochoa et al., 2010), despite the fact that there are no reports to use Hedgehog for hepatic differentiation of human ES/iPS cells.

There have been many reports to show *in vitro* differentiation of human ES/iPS cells toward hepatocytes, although most of the studies utilizes animal-derived cells and/or materials during at least one step of differentiation cultures (Agarwal et al., 2008; Cai et al., 2007; Chiao et al., 2008; Duan et al., 2007, 2010; Hay et al., 2008a, 2008b; Inamura et al., 2011; Ishii et al., 2008; Liu et al., 2010; Mfopou et al., 2010; Sasaki et al., 2009; Si-Tayeb et al., 2010; Song et al., 2009; Sullivan et al., 2010; Touboul et al., 2010; Zhao et al., 2009), such as the presence of MEF or MEF-conditioned medium at the initial step of the culture, the presence of mouse feeder cells for differentiation induction, or fetal bovine serum during the certain periods of differentiation culture. In

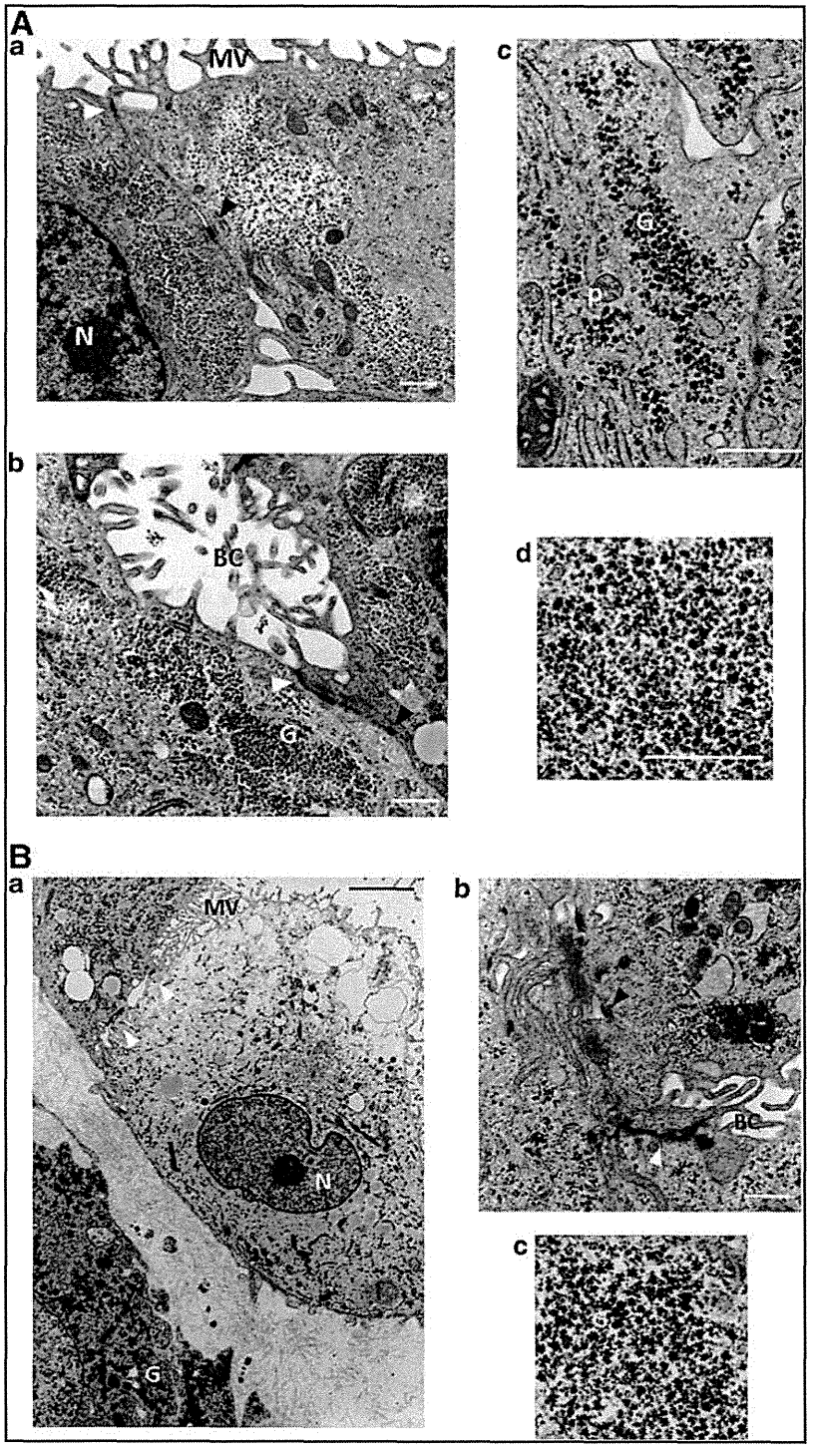

FIG. 5. Transmission electron micrographs of hepatocyte and cholangiocytes induced from human ES and iPS cells. (**A**) Hepatocytes derived from human ES cells (KhES-1 cells). (a) apical surface microvilli (MV), tight-junction (white arrowhead), desmosome (black arrowhead), and nucleus (N). (b) bile canaliculus (BC), glycogen granule (G), tight-junction (white arrowhead) and desmosome (black arrowhead). (c) glycogen granule (G) and peroxisome (p). (d) rosette formation of glycogen granules. (**B**) Hepatocytes derived from human iPS cells (SeV5) (a) apical surface microvilli (MV), glycogen granule (G), and nucleus (N). (b) bile canaliculus (BC), tight-junction (white arrowhead) and desmosome (black arrowhead). (c) rosette formation of glycogen granules. (**C**) Cholangiocytes derived from human iPS cells ((a) #40 cells and (b) SeV5 cells). Bile duct lumen (BD) side with short microvilli (white arrowhead) and outer side with basement membrane (black arrowhead). N: nucleus. White scale bar = 2 μm, and black scale bar = 10 μm.

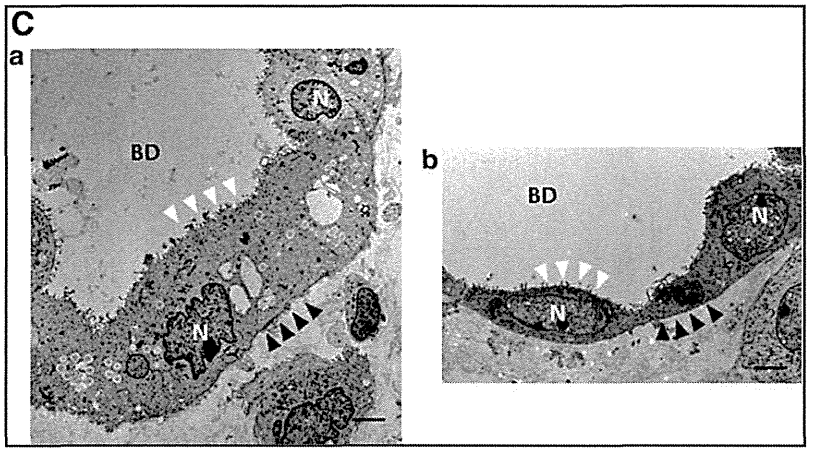

FIG. 5. (Continued).

contrast, the only xenogeneic materials used in our differentiation protocol were Matrigel and KSR, both of which may be substituted by equivalent products of human origin. The present results contribute to the development of production techniques for human hepatocytes free from animal products and a good product level.

In this study, we succeeded in inducing functional hepatocytes from several human pluripotent stem cells with distinct origins and diverse characteristics. We used human iPS cells from adult fibroblast, neonatal fibroblasts, and fetal fibroblasts and in addition human ES cells. Induction methods of iPS cells also varied, that is, traditional retrovirus vector and Sendai virus vector. Despite these variations, we were able to reproduce stable and effective differentiation in all situations. Thus, our differentiation-inducing method is universal and might be widely applicable.

Human iPS cells were originally been established using retrovirus and lentivirus vectors (Park et al., 2008; Takahashi and Yamanaka, 2006; Takahashi et al., 2007; Yu et al., 2007), and these methods for iPS induction have been of major concern for the clinical application of iPS cells. On the other hand, RNA-based methods (Warren et al., 2010), including SeV vectors (Ban et al., 2011; Fusaki et al., 2009) are really hopeful and lead to a reproducible supply of safe human iPS cells. In this study, using Sendai virus vectors and our efficient differentiation methods, we succeeded in genome virus free production of human mature hepatocyte from safe human iPS cells.

We demonstrated sufficient induction of CYP3A4 in differentiated hepatocytes at the levels of mRNA, protein and activity. It is well known that many drugs are metabolized by CYP3A4 and many drugs inhibit its activity, and furthermore several drugs induce its expression (Liu et al., 2007). In this study, we observed an additional induction of CYP3A4 by dexamethasone. These findings suggest the physiological functionality of hepatocytes derived from human pluripotent stem cells in the present study and usefulness of these differentiated cells as *in vitro* drug metabolic studies.

In addition to CYP3A4, we demonstrated the induction of AAT at the protein level in human hepatocytes induced from human pluripotent stem cells, and this protein was not detected in control human hepatocytes used as positive control. In this point, therefore, human hepatocytes derived from human ES/iPS cells via our culture system are superior to the commercial human hepatocytes used so far. AAT is an inhibitor for proteinase and is thought to play an important role in regulating a wide variety of proteolytic reactions in the human body. Congenital deficiency of this enzyme is associated with serious lung and liver damage, and Rashid et al. (2010) reported the establishment of patient-specific iPS cells of this enzyme deficiency. Thus, our culture system may contribute to the analysis of this congenital disease. In contrast to CYP3A4, AAT is released from hepatocytes into the bloodstream after being produced. Thus, we believe that human hepatocytes generated using the present culture protocol have full capacity to produce two important functional proteins working inside and outside the liver, and thereby contributing homeostasis in the human body.

In the present study, we clarified that hepatocytes differentiated from human pluripotent stem cells could be useful for *in vitro* hepatocyte cytotoxicity assays. Unlike the results of previous studies that showed an *in vitro* apoptosis-related phenomenon (Bao et al., 2010) and extracellular release of total LDH (Siendones et al., 2005) and/or performed in *in vivo* animal studies (Kuhla et al., 2009), we identified the extracellular release of hepatocyte-specific enzymes, such as GOT and hepatocyte-specific isozymes of LDH, using *in vitro* human culture systems. In addition, we also showed that the cytotoxicity was really specific for hepatocytes because cytotoxicity was not or only minimally observed in the cells other than hepatocytes including undifferentiated human pluripotent stem cells and HUVEC. These results are the first demonstration of hepatocyte-specific cytotoxicity particularly in induced cells derived from human pluripotent stem cells, and the convenient *in vitro* assay system might be applicable to various *in vitro* testing approaches for substances that are toxic to the liver. In addition, our cytotoxic assay might also be used for cytotoxicity assays for epithelial cells of the biliary tract, because extracellular release of γ-GTP and LAP were detected upon cytotoxic stimulation. This toxicity of hepatocytes (and probably biliary epithelial cells) was attenuated by hepatoprotective PGE1, showing a possible therapeutic model of human liver damage, because PGE1 is a

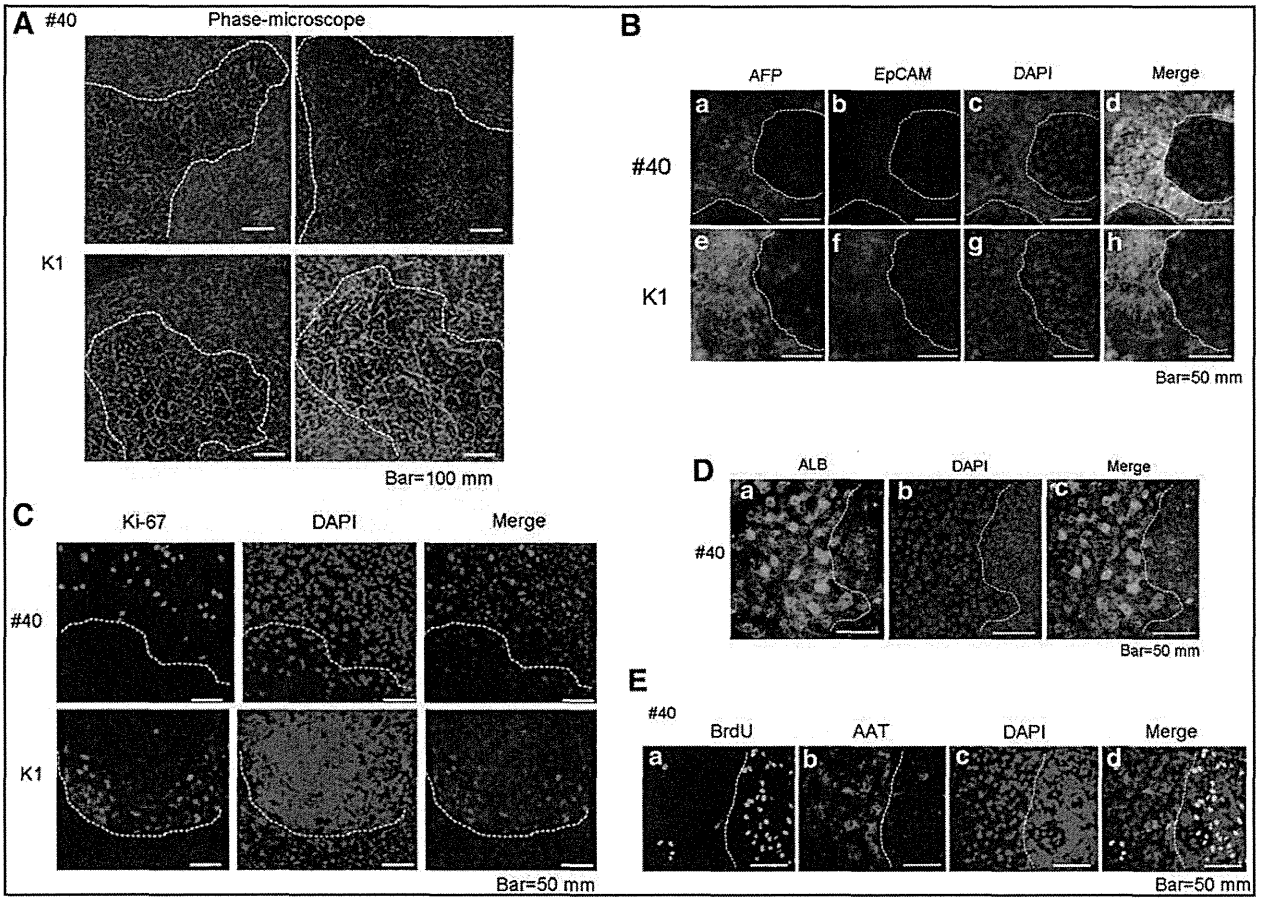
A
#40
Phase-microscope
K1
Bar=100 mm
B
AFP
EpCAM
DAPI
Merge
#40
K1
Bar=50 mm
C
Ki-67
DAPI
Merge
#40
K1
Bar=50 mm
D
ALB
DAPI
Merge
#40
Bar=50 mm
E
#40
BrdU
AAT
DAPI
Merge
Bar=50 mm

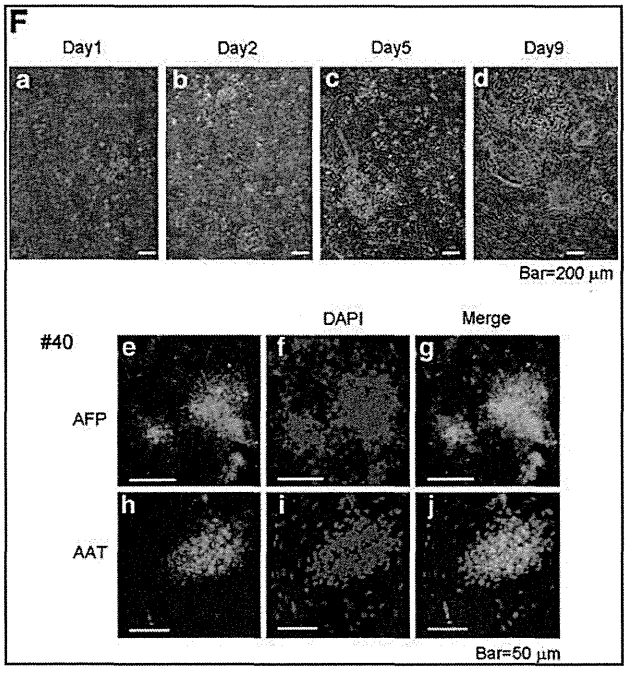
F
Day1
Day2
Day5
Day9
Bar=200 μm
DAPI
Merge
#40
AFP
AAT
Bar=50 μm

FIG. 6. Immature proliferating and mature hepatocyte fractions in induced cells. (**A**) Phase contrast microscopy of hepatocytes induced from human iPS cells (#40 cells) and ES cells (K1: KhES-1 cells) (on the 29th day of differentiation culture). A flattened area containing abundant binuclear cells is surrounded by an area of immature proliferating cells with a bulging cell clump. The border lines of these two areas are indicated by dotted lines. Scale bar = 100 μm. (**B**) Immunostaining of hepatocyte-specific markers of hepatocytes induced from human iPS cells (#40 cells) (upper panel, a, b, c, and d) and ES cells (K1: KhES-1 cells) (lower panel, e, f, g, and h) (on the 29th day of differentiation culture). Cells were stained using a rabbit polyclonal antihuman α-fetoprotein (AFP) antibody and a mouse monoclonal antihuman epithelial cell adhesion molecule (EpCAM) antibody as indicated. DAPI (1 μg/mL) was used to stain the cell nucleus. In each subfigure, right-side or lower side images show flattened monolayer areas and that are negative or weakly positive for AFP and EpCAM, whereas left-side images show bulging cell clump areas that are strongly positive for AFP and EpCAM. The border lines of these two areas are indicated by dotted lines. Scale bar = 50 μm. (**C**) BrdU incorporation and immunostaining of Ki-67, proliferation marker, of hepatocytes induced from human iPS cells (#40 cells) (upper panel, a and b) and ES cells (K1: KhES-1 cells) (lower panel, c and d) (on the 29th day of differentiation culture). Cells were labeled with fluorescent BrdU or stained with a rabbit polyclonal antihuman Ki-67 antibody as indicated. DAPI (1 μg/mL) was used to stain the cell nucleus. In each subfigure, upper side (a, b, and d) or lower side (c) images show bulging cell clump areas that are positive for BrdU uptake and Ki-67. The border lines of these two areas are indicated by dotted lines. Scale bar = 50 μm. (**D**) Immunostaining of albumin (ALB) of hepatocytes induced from human iPS cells (#40 cells) on the 29th day of differentiation culture. Cells were stained with a rabbit polyclonal antihuman ALB antibody as indicated. DAPI (1 μg/mL) was used to stain the cell nucleus. In each subfigure, left-side images show flattened monolayer areas that are positive for ALB, whereas right-side images show bulging cell clump areas that are negative or only weakly positive for ALB. The border lines of these two areas were indicated by dotted lines. Scale bar = 50 μm. (**E**) Incorporation of BrdU and immunostaining of α1-antitrypsin (AAT) of hepatocytes induced from human iPS cells (#40 cells) on the 29th day of differentiation culture. Cells were labeled with fluorescent BrdU and stained with a rabbit polyclonal antihuman AAT antibody as indicated. DAPI (1 μg/mL) was used to stain the cell nucleus. In each subfigure, left-side images show bulging cell clump areas that are positive for BrdU uptake, whereas right-side images show flattened monolayer areas that are positive for AAT. The border lines of these two areas are indicated by dotted lines. Scale bar = 50 μm. (**F**) Passage and regrowth of hepatocytes induced from human iPS cells (#40 cells) in the new culture dish. On the 28th day of differentiation culture, induced hepatocytes were collected from the original culture dishes and were recultured in new collagen-coated dishes. On the second day of reculture in the new dishes, colonies of small-sized cells appeared (red arrows), and these colonies expanded during the reculturing for up to 9 days (upper panel). Immunostaining of AFP and AAT were performed using specific antibodies (lower panel).

candidate hepatoprotective agent also in the clinical settings (Hara et al., 2010).

In our differentiation-inducing culture system, not only hepatocytes but also cholangiocytes seems to be induced concomitantly, as suggested by the cytotoxic study described above. These findings were confirmed by morphological studies using electron microscopy. It is well known that both hepatocytes and cholangiocytes are derived from common precursor cells called "hepatoblasts" (Zhao and Duncan, 2005). Because the differentiated cell in our culture system expressed AFP, it is likely that our culture system contains hepatoblasts even at the terminal stage of differentiation. In the present study, we identified AFP and EpCAM double-positive cells in our culture system and these cells were also positive for Ki-67 and BrdU, suggesting the presence of hepatocyte progenitors with high proliferative potential. We also showed that induced cells were passageable and did proliferate again in new dishes. In addition, proliferating cells (colony-forming small-sized cells) in the new dish continued to express hepatocyte markers. These smaller hepatocytes with proliferating potential might be a human counterpart of rat small hepatocyte progenitor cells (Chen et al., 2007; Mitaka et al., 1992, 1995). We propose a possible *in vivo* functional reconstitution of liver with a bile acid delivering system to the bloodstream by transplanting simultaneously hepatocyte and cholangiocytes together with endothelial cells induced from human pluripotent stem cells, because we also succeeded in highly efficient endothelial induction from human ES/iPS cells (Gokoh et al., 2011; Nakahara et al., 2009a).

In this study, we used HepaRG cells as one of the control hepatocyte. This cell line has originally been established from hepatocytes in patients with type C hepatitis, but was free of hepatitis virus. In addition, HepaRG cells express a large panel of liver-specific genes, including those expressing drug metabolizing enzymes and therefore were widely used as human hepatocyte model in many recent reports (Guguen-Guillouzo and Guillouzo, 2010; Marion et al. 2010). Despite this, there are no reports with this cell line of hepatocyte induction from human ES/iPS cells. We could show that hepatocyte-like cells induced from human pluripotent stem cells via our culture system were almost equivalent or potentially superior to this standard hepatocyte.

In the present study, we presented novel efficient method to produce functional hepatocytes from pluripotent stem cells. In regard to the possible methods for hepatocyte production, there is another important option, namely, direct reprogramming from somatic cells. Recent two reports (Huang et al., 2011; Sekiya and Suzuki, 2011) clearly showed the usefulness of this strategy, and proposed several defined factors for direct induction of hepatocytes from fibroblasts, which may be also useful for differentiation induction of hepatocytes from pluripotent stem cells. However, mouse cells and retrovirus and/or lentivirus vectors were used in these two reports. Further studies using human cells and more safe vectors are necessary for the clinical application of this powerful method.

Author Disclosure Statement

The authors declare that no conflicting financial interests exist.

References

Agarwal, S., Holton, K.L., and Lanza, R. (2008). Efficient differentiation of functional hepatocytes from human embryonic stem cells. Stem Cells 26, 1117–1127.

Ban, H., Nishishita, N., Fusaki, N., et al. (2011). Efficient generation of transgene-free human induced pluripotent stem cells (iPSCs) by temperature-sensitive Sendai virus vectors. Proc. Natl. Acad. Sci. USA, in press.

Bao, X.Q. and Liu, G.T. (2010). Bicyclol protects HepG2 cells against D-galactosamine-induced apoptosis through inducing heat shock protein 27 and mitochondria associated pathway. Acta Pharmacol. Sinica 31, 219–226.

Cai, J., Zhao, Y., Liu, Y., et al. (2007). Directed differentiation of human embryonic stem cells into functional hepatic cells. Hepatology 45, 1229–1239.

Chen, Q., Kon, J., Ooe, H., et al. (2007). Selective proliferation of rat progenitor cells in serum free culture. Nat. Protoc. 2, 1197–1205.

Chiao, E., Elazar, M., Xiong, A., et al. (2008). Isolation and transcriptional profiling of purified hepatic cells derived from human embryonic stem cells. Stem Cells 26, 2032–2041.

Duan, Y., Catana, A., Meng, Y., et al. (2007). Differentiation and enrichment of Hepatocyte-like cells from human embryonic stem cells *in vitro* and *in vivo*. Stem Cells 25, 3058–3068.

Duan, Y., Ma, X., Zou, W., et al. (2010). Differentiation and characterization of metabolically functioning hepatocytes from human embryonic stem cells. Stem Cells 28, 674–686.

Fusaki, N., Ban, H., Nishiyama, A., et al. (2009). Efficient induction of transgene-free human pluripotent stem cells using a vector based on Sendai virus, an RNA virus that does not integrate into the host genome. Proc. Jpn. Acad., Ser. B, Phys. Biol. Sci. 85, 348–362.

Ghadially, F.N. (1997). *Ultrastructural Pathology of the Cell and Matrix*. (Butterworth–Heinemann, Boston, MA), pp. 1–1414.

Gokoh, M., Nishio, M., Nakamura, N., et al. (2011). Early senescence is not an inevitable fate of human induced pluripotent stem-derived cells. Cell. Reprogram. 13, 361–370.

Gripon, P., Rumin, S., Urban, S., et al. (2002). Infection of a human hepatoma cell line by hepatitis B virus. Proc. Natl. Acad. Sci. USA 99, 15655–15660.

Guguen-Guillouzo, C., and Guillouzo, A. (2010). General review on *in vitro* hepatocyte models and their applications. Methods Mol. Biol. 640, 1–40.

Hara, Y., Akamatsu, Y., Kobayashi, Y., et al. (2010). Perfusion using oxygenated buffer containing prostaglandin E1 before cold preservation prevents warm ischemia-reperfusion injury in liver grafts from heart-beating donors. Transplant. Proc. 42, 3973–3976.

Hay, D.C., Fletcher, J., Payne, C., et al. (2008a). Highly efficient differentiation of hESCs to functional hepatic endoderm requires ActivinA and Wnt3a signaling Proc. Natl. Acad. Sci. USA 105, 12301–12306.

Hay, D.C., Zhao, D., Fletcher, J., et al. (2008b). Efficient differentiation of hepatocytes from human embryonic stem cells exhibiting recapitulating liver development *in vivo*. Stem Cells 26, 894–902.

Hirose, Y., Itoh, T., and Miyajima, A. (2009). Hedgehog signal activation coordinates proliferation and differentiation of fetal liver progenitor cells. Exp. Cell Res. 315, 2648–2657.

Huang, P., He, Z., Ji, S., et al. (2011). Induction of functional hepatocyte-like cells from mouse fibroblasts by defined factors. Nature 475, 386–389.

Inamura, M., Kawabata, K., Takayama, K., et al. (2011). Efficient generation of hepatoblasts from human ES cells and iPS cells by transient overexpression of homeobox gene HEX. Mol. Ther. 19, 400–407

Ishii, T., Fukumitsu, K., Yasuchika, K., et al. (2008). Effects of extracellular matrixes and growth factors on the hepatic differentiation of human embryonic stem cells. Am. J. Physiol. Gastrointest. Liver Physiol. 295, G313–G321.

Kuhla, A., Eipel, C., Abshagen, K., et al. (2009). Role of perforin/granzyme cell death pathway in D-Gal/LPS-induced inflammatory liver injury. Am. J. Physiol. Gastrointest. Liver Physiol. 296, G1069–G1076.

Liu, H., Ye, Z., Kim, Y., et al. (2010). Generation of endoderm-derived human induced pluripotent stem cells from primary hepatocytes. Hepatology 51, 1810–1819.

Liu, Y.T., Hao, H.P., Liu, C.X., et al. (2007). Drugs as CYP3A4 probes inducers, and inhibitors. Drug Metab. Rev. 39, 699–721.

Marion, M.J., Hantz, O., and Durantel, D. (2010). The HepaRG cell line: biological properties and relevance as a tool for cell biology, drug metabolism, and virology studies. Methods Mol. Biol. 640, 261–272.

Mfopou, J.K., Chen, B., Mateizel, I., et al. (2010). Noggin, retinoids, and fibroblast growth factor regulate hepatic or pancreatic fate of human embryonic stem cells. Gastroenterology 138, 2233–2245.

Miro, J.M., Laguno, M., Moreno, A., et al. (2006). Management of end stage liver disease (ESLD): what is the current role of orthotopic liver transplantation (OLT)? J. Hepatol. 44, S140–S145.

Mitaka, T., Mikami, M., Sattler, G.L., et al. (1992). Small cell colonies appear in the primary culture of adult rat hepatocytes in the presence of nicotinamide and epidermal growth factor. Hepatology 16, 440–447.

Mitaka, T., Kojima, T., Mizuguchi, T., et al. (1995). Growth and maturation of small hepatocytes isolated from adult rat liver. Biochem. Biophys. Res. Commun. 214, 310–317.

Nagata, S., Toyoda, M., Yamaguchi, S., et al. (2009). Efficient reprogramming of human and mouse primary extra-embryonic cells to pluripotent stem cells. Genes Cells 14, 1395–1404.

Nakahara, M., Nakamura, N., Matsuyama, S., et al. (2009a). High efficiency production of subculturable vascular endothelial cells from feeder-free human embryonic stem cells without cell-sorting technique. Cloning Stem Cells 11, 509–522.

Nakahara, M., Saeki, K., Nakamura, N., et al. (2009b). Human embryonic stem cells with maintenance under a feeder-free and recombinant cytokine-free condition. Cloning Stem Cells 11, 5–18.

Ochoa, B., Syn, W.K., Delgado, I., et al. (2010). Hedgehog signaling is critical for normal liver regeneration after partial hepatectomy in mice. Hepatology 51, 1712–1723.

Park, I.H., Zhao, R., West, J.A, et al. (2008). Reprogramming of human somatic cells to pluripotency with defined factors. Nature 451, 141–146.

Rashid, S.T., Corbineau, S., Hannan, N., et al. (2010). Modeling inherited metabolic disorders of the liver using human induced pluripotent stem cells. J. Clin. Invest. 120, 3127–3136.

Saeki, K., Saeki, K., Nakahara, M., et al. (2009) A feeder-free and efficient production of functional neutrophils from human embryonic stem cells. Stem Cells 27, 59–67.

Sasaki, K., Ichikawa, H., Takei, S., et al. (2009). Hepatocyte differentiation from human ES cells using simple embryoid body formation method and the staged- additional cocktail. Sci. World J. 9, 884–890.

Schmelzer, E., Wauthier, E., and Reid, L.M. (2006) The phenotypes of pluripotent human hepatic progenitors. Stem Cells 24, 1852–1858.

Sekiya, S., and Suzuki, A. (2011). Direct conversion of mouse fibroblasts to hepatocyte-like cells by defined factors. Nature 475, 390–393.

Siendones, E., Jimeneze-Gomez, Y., Montero, J.L., et al. (2005). PGE_1 abolishes the mitochondrial-independent cell death pathway induced by D-galactosamine in primary culture of rat hepatocytes. J. Gastroenterol. Hepatol. 20, 108–116.

Si-Tayeb, K., Noto, F.K., Nagaoka, M., et al. (2010). Highly efficient generation of human hepatocyte-like cells from induced pluripotent stem cells. Hepatology 51, 297–305.

Song, Z., Cai, J., Liu, Y., et al. (2009). Efficient generation of hepatocyte-like cells from human induced pluripotent cells. Cell Res. 1, 1–10.

Suemori, H., Yasuchika, K., Hasegawa, K., et al. (2006). Efficient establishment of human embryonic stem cell lines and long-term maintenance with stable karyotype by enzymatic bulk passage. Biochem. Biophys. Res. Commun. 345, 926–932.

Sullivan, G.J., Hay, D.C., Park, I.H., et al. (2010). Generation of functional human hepatic endoderm from human induced pluripotent stem cells. Hepatology 51, 329–335.

Takahashi, K., and Yamanaka, S. (2006). Induction of pluripotent stem cells from mouse embryonic and adult fibroblast cultures by defined factors. Cell 126, 663–676.

Takahashi, K., Tanabe, K., Ohnuki, M., et al. (2007). Induction of pluripotent stem cells from adult human fibroblasts by defined factors. Cell 131, 861–872.

Thomson, J.A., Itskovitz-Eldor, J., Shapiro, S.S., et al. (1998). Embryonic stem cell lines derived from human blastocysts. Science 282, 1145–1147.

Touboul, T., Hannan, N.R.F., Corbineau, S., et al. (2010). Generation of functional hepatocytes from human embryonic stem cells under chemically defined conditions that recapitulate liver development. Hepatology 51, 1754–1765.

Toyoda, M., Yamazaki-Inoue, M., Itakura, Y., et al. (2011). Lectin microarray analysis of pluripotent and multipotent stem cells. Genes Cells 16, 1–11.

Warren, L., Manos, P.D., Ahfeldt, T., et al. (2010). Highly efficient reprogramming to pluripotency and directed differentiation of human cells with synthetic modified mRNA. Cell Stem Cell 7, 1–13.

Yu, J., Vodyanik, M.A,, Smuga-Otto, K., et al. (2007). Induced pluripotent stem cell lines derived from human somatic cells. Science 318, 1917–1920.

Zhao, D., Chen, S., Cai, J., et al. (2009). Derivation and characterization of hepatic progenitor cells from human embryonic stem cells. PLoS One 4, 1–10.

Zhao, R., and Duncan, S.A. (2005) Embryonic development of the liver. Hepatology 41, 956–967.

Address correspondence to:
Akira Yuo, M.D., Ph.D.
Department of Disease Control
Research Institute,
National Center for Global Health and Medicine
1-21-1, Toyama, Shinjuku-ku
Tokyo 162-8655, Japan

E-mail: yuoakira@ri.ncgm.go.jp

Cell Metabolism
Resource

Production of Functional Classical Brown Adipocytes from Human Pluripotent Stem Cells using Specific Hemopoietin Cocktail without Gene Transfer

Miwako Nishio,[1] Takeshi Yoneshiro,[4] Masako Nakahara,[1] Shinnosuke Suzuki,[1] Koichi Saeki,[5] Mamoru Hasegawa,[5] Yuko Kawai,[6] Hidenori Akutsu,[7] Akihiro Umezawa,[7] Kazuki Yasuda,[2] Kazuyuki Tobe,[8] Akira Yuo,[1] Kazuo Kubota,[3] Masayuki Saito,[9] and Kumiko Saeki[1,*]
[1]Department of Disease Control, Research Institute
[2]Department of Metabolic Disorder, Diabetes Research Center, Research Institute
[3]Department of Radiology
National Center for Global Health and Medicine, Tokyo 162-8655, Japan
[4]Laboratory of Histology and Cytology, Department of Anatomy, Hokkaido University Graduate School of Medicine, Sapporo 060-8638, Japan
[5]DNAVEC Corporation, Ibaraki 300-2511, Japan
[6]LSI Sapporo Clinic, Sapporo 065-0013, Japan
[7]Department of Reproductive Biology, Center for Regenerative Medicine, National Research Institute for Child Health and Development, Tokyo 157-8535, Japan
[8]The First Department of Internal Medicine, Faculty of Medicine, University of Toyama, Toyama 930-0194, Japan
[9]Department of Nutrition, School of Nursing and Nutrition, Tenshi College, Sapporo 065-0013, Japan
*Correspondence: saeki@ri.ncgm.go.jp
http://dx.doi.org/10.1016/j.cmet.2012.08.001

SUMMARY

Brown adipose tissue is attracting much attention due to its antiobestic effects; however, its development and involvement in metabolic improvement remain elusive. Here we established a method for a high-efficiency (>90%) differentiation of human pluripotent stem cells (hPSCs) into functional classical brown adipocytes (BAs) using specific hemopoietin cocktail (HC) without exogenous gene transfer. BAs were not generated without HC, and lack of a component of HC induced white adipocyte (WA) marker expressions. hPSC-derived BA (hPSCdBA) showed respiratory and thermogenic activation by β-adrenergic receptor (AdrRβ) stimuli and augmented lipid and glucose tolerance, whereas human multipotent stromal cell-derived WA (hMSCdWA) improved lipid but inhibited glucose metabolism. Cotransplantation of hPSCdBA normalized hMSCdWA-induced glucose intolerance. Surprisingly, hPSCdBAs expressed various hemopoietin genes, serving as stroma for myeloid progenitors. Moreover, AdrRβ stimuli enhanced recovery from chemotherapy-induced myelosuppression. Our study enhances our understanding of BA, identifying roles in metabolic and hemogenic regulation.

INTRODUCTION

Brown adipose tissue (BAT) is involved in nonshivering thermogenesis during cold exposure (Enerbäck et al., 1997) and diet-induced thermogenesis (Feldmann et al., 2009). It also contributes to the prevention of aging-associated obesity, as demonstrated in *Ucp1* null mice (Kontani et al., 2005). In large-sized mammals, the majority of BAT disappears within a few days after birth; however, some portions remain and function through adulthood. ^{18}Fluorodeoxyglucose-positron emission tomography in combination with computed tomography (^{18}F-FDG-PET/CT) along with histological and gene expressional studies has shown the presence of functional BAT in adult humans in supraclavicular and paravertebral regions (Cypess et al., 2009; Virtanen et al., 2009; van Marken Lichtenbelt et al., 2009; Saito et al., 2009; Yoneshiro et al., 2011). Although accumulating evidence has shown an inverse correlation between the amounts of active BAT and the development of metabolic syndrome in humans (Ouellet et al., 2011; Jacene et al., 2011), the cause-and-effect relationship between BAT and metabolic improvement remains unsubstantiated. Moreover, the whole picture of the development of human BAT is not clarified yet; for example, it remains elusive whether BAT derives from a common progenitor with myoblast, immature mesenchymal cells from which white adipocyte (WA) is also generated or from vascular components such as endothelial and perivascular cells (Tran et al., 2012; Gupta et al., 2012), and whether bone morphogenic protein 7 (BMP7) (Tseng et al., 2008) is sufficient or additional cytokines are required for BA differentiation. The newly proposed concept of brite adipocytes, WA-derived BA-like cells (*br*own + wh*ite* = brite) (Petrovic et al., 2010), makes the situation complex, often encumbering an understanding of classical BAT development. For an advanced understanding of BAT, establishing a method to generate BAs from pluripotent stem cells, including embryonic stem cells (ESCs) and induced pluripotent stem cells (iPSCs), is of great use. Recently, a trial to program human iPSCs (hiPSCs) into BA via transferring of exogenous genes was reported (Ahfeldt et al., 2012); however, biological effects of the programmed BA on lipid/glucose metabolism remains unevaluated. Moreover, artificially programmed

cells are not applicable to the investigations on natural developmental pathways of human BA.

The existence of BAT in bone marrow (BM), which attenuates with aging and diabetes, was reported in mice (Krings et al., 2012). Also, a nontumorous infiltration of BAT in human BM was reported in a case of essential hyperthrombocythemia (Thorns et al., 2008). A functional link between BM fat and hematopoiesis was first reported by Dexter et al. (Dexter et al., 1977), who showed that BM adipocytes with mitochondria-attached multilocular lipid droplets were essential for the maintenance of colony-forming units-spleen (CFU-S), a short-term repopulating hematopoietic progenitor cell (HPC) distinct from hematopoietic stem cell (HSC). Although the microenvironment for HSC (reviewed in Kiel and Morrison, 2006; Arai and Suda, 2007) and B cells (Nagasawa, 2007) has been intensively studied, that for myeloid progenitor cells (MPCs) remains poorly understood. Moreover, controversial findings have been reported regarding the effects of "BM adipocyte" on the committed HPCs: some reports showed its capacity to support lymphopoiesis (Gimble et al., 1990) and granulopoiesis (Gimble et al., 1992), while others showed its inhibiting effects for hematopoiesis (Ookura et al., 2007, Naveiras et al., 2009). The controversy may come from, at least in part, the heterogeneity of bone marrow fat cells including BAT versus white adipocyte tissue (WAT).

During our research into the feeder-free hematopoietic differentiation of hPSCs, we serendipitously found the existence of BA-like cell clusters surrounding the hematopoietic centers and an induction of BA-selective gene, *PRDM16* (see Figure S1 online). Because the hematopoietic differentiation was achieved under a completely feeder-free condition, a de novo hematopoietic stroma must be generated from hPSCs per se. Eventually, murine C3H10T1/2 line, a commonly used feeder for the hematopoietic differentiation of monkey (Hiroyama et al., 2006) and human (Takayama et al., 2008) ESCs, can differentiate into functional BA (Tseng et al., 2008). Thus, an association between BA development and hemopoiesis has been suggested.

After a process of trial and error, we established a high-efficiency method to produce functional BAs from hPSCs including human ESCs (hESCs) and hiPSCs. Involvement of hPSC-derived BAs (hPSCdBAs) in metabolic improvement, its service as a stroma for MPCs, and the existence of BA in vertebral BM are also shown.

RESULTS

Directed Differentiation of Human PSC into Functional BA

By utilizing a specific hemopoietin cocktail (HC) composed of KIT ligand (KITLG), fms-related tyrosine kinase 3 ligand (FLT3LG), interleukin-6 (IL-6), and vascular endothelial growth factor (VEGF) along with the previously reported BA inducer BMP7 (Tseng et al., 2008), we successfully established a highly efficient BA differentiation method for hESCs and hiPSCs (Supplemental Information). The differentiated cells exclusively contained multilocular lipid droplets (Figure 1A), as confirmed by oil red O staining (Figure 1B). Quantitative RT-PCR studies demonstrated the induction of BAT-specific genes of *UCP1* and *PRDM16*, which were not detected in human multipoint stromal cell-derived WA (hMSCdWA) (Figure 1C). Although depletion of BMP7 significantly lowered BA differentiation efficiency as reported by Tseng et al. (Tseng et al., 2008) (Figure S2), BA differentiation was completely abolished by HC depletion even in the presence of BMP7 (Figure 1D). Expression of a series of BAT-selective and BAT/WAT-common genes, but not WAT-selective genes, was also determined (Figure 1E). UCP1 protein expression was confirmed by immunostaining studies, showing that over 95% of the BA differentiated cells expressed UCP1 at mitochondria (Figure 2A), and also western blotting, showing the presence of a 32 kDa band in the differentiated cells (Figure 2B). Lipid staining illustrated the wide distribution of mitochondria within the cytosol, some of which resided close to lipid droplets (Figure 2C). Electron micrographs confirmed the presence of multilocular lipid droplets and abundant mitochondria rich in transverse cristae (Figure 2D and Figure S3A), some of which located in close vicinity to lipid droplets (Figure S3B), in contrast to hMSCdWA, which showed meager mitochondria (Figure S3C).

We next evaluated the functional maturation of hESC/hiPSC-derived BAs. First, thermogenic potential was evaluated. Treatment with a β-adrenergic receptor, isoproterenol, augmented the expression of *UCP1*, a major contributor to thermogenesis, and *PRDM16*, a major inducer of *UCP1* expression, in hPSCdBAs (Figures 3A and 3B, left). Isoproterenol-responsive thermogenic activation (Jackson et al., 2001) was further confirmed in vivo by subcutaneous transplantation of hPSCdBAs into mice (Figures 3A and 3B, right). Respiratory activation was also assessed in vitro: hPSCdBAs showed considerably higher basal and maximum OCRs than hMSCdWA as demonstrated by a standard Mito Stress Test (Figure 3C). Responsiveness to a β3-adrenergic receptor-selective agonist, CL316,243, was also determined: statistically significant upregulation in oxygen consumption rates (OCRs) was determined in the cases of hPSCdBAs in response to CL316,243, whereas no significant changes were observed in the cases of hMSCdWA and immature hPSCs (Figure 3D). Upregulation of OCR was further determined in isoproterenol-treated hPSCdBAs (data not shown).

Together, these findings support the production of functional BAs from hPSCs.

Effects of hPSC-Derived BA on Lipid and Glucose Metabolism

Because endogenous BAT reportedly reduces blood triglyceride (TG) levels in response to cold stimuli (Bartelt et al., 2011), we examined the effects of transplantation of hPSCdBA on lipid metabolism. Compared to immature hPSC-transplanted mice, hPSCdBA-transplanted mice (Figure 4A, middle column) and hMSCdWA-transplanted mice (Figure 4A, right column) showed reduced fasting TG levels. Olive oil tolerance tests further confirmed that hPSCdBA transplantation augmented resistance to oral lipid loading (Figure 4B).

Next, effects of hPSCdBAs on glucose metabolism were evaluated. Ten-week-old mice were subcutaneously injected with saline, hESC-derived BA (hESCdBA), or hMSCdWA, and blood glucose levels were measured over time (Figure 4C). Fasting blood glucose levels were significantly lowered in hESCdBA-transplanted mice compared to saline-injected mice ($p = 0.0032$; $n = 3$) and to hMSCdWA-transplanted mice ($p = 0.0030$;

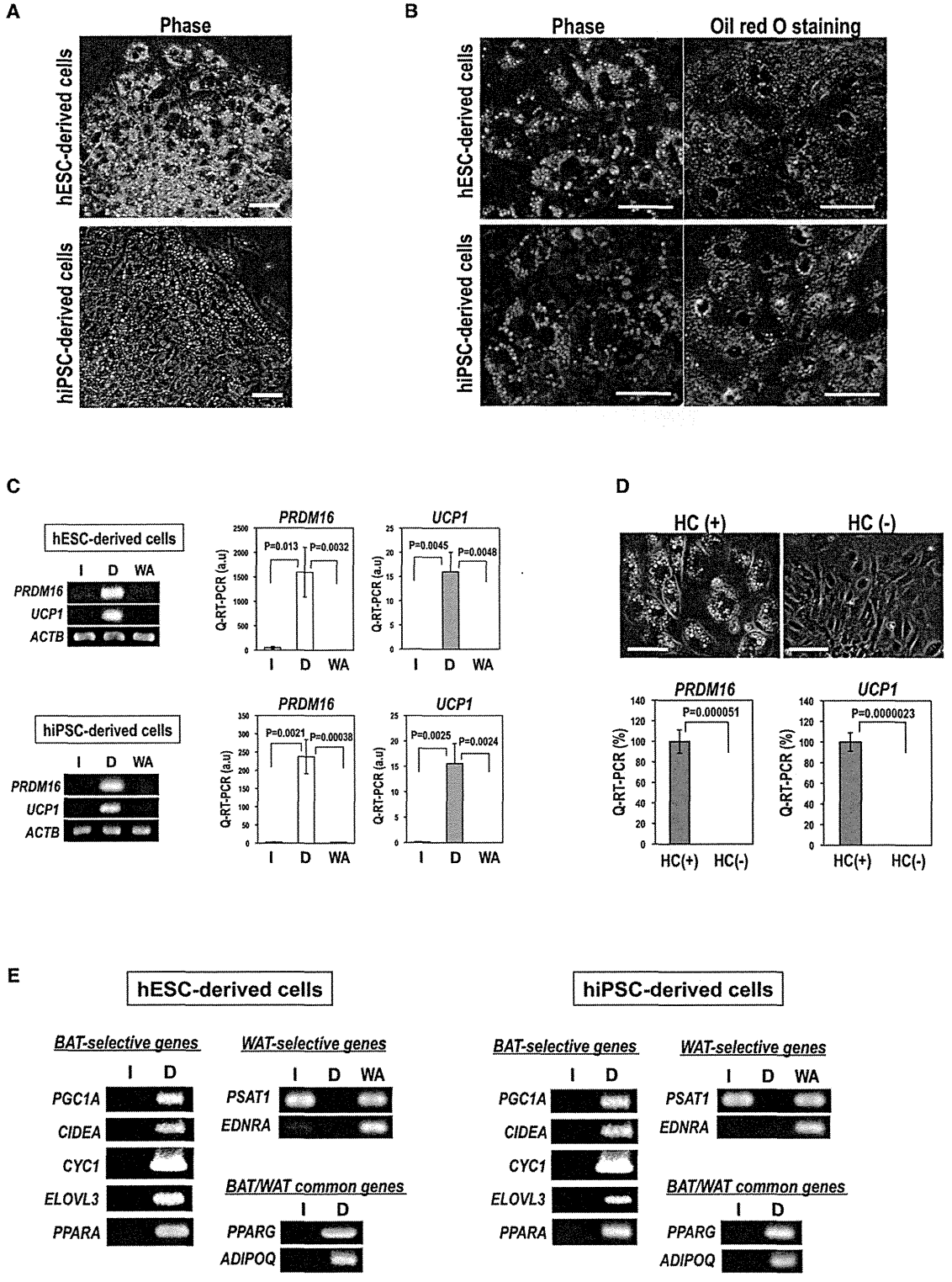

Figure 1. Differentiation of hPSCs into BAs

(A) Microscopy of hPSC-derived cells. Scale bar, 50 μm.

(B) Oil red O staining (right) with phase contrast microscopy (left). Scale bar, 40 μm.

(C) Expression of *PRDM16* and *UCP1* determined by RT-PCR (left) or real-time PCR (middle and right). The error bars represent average ± standard deviation (SD) (n = 3).

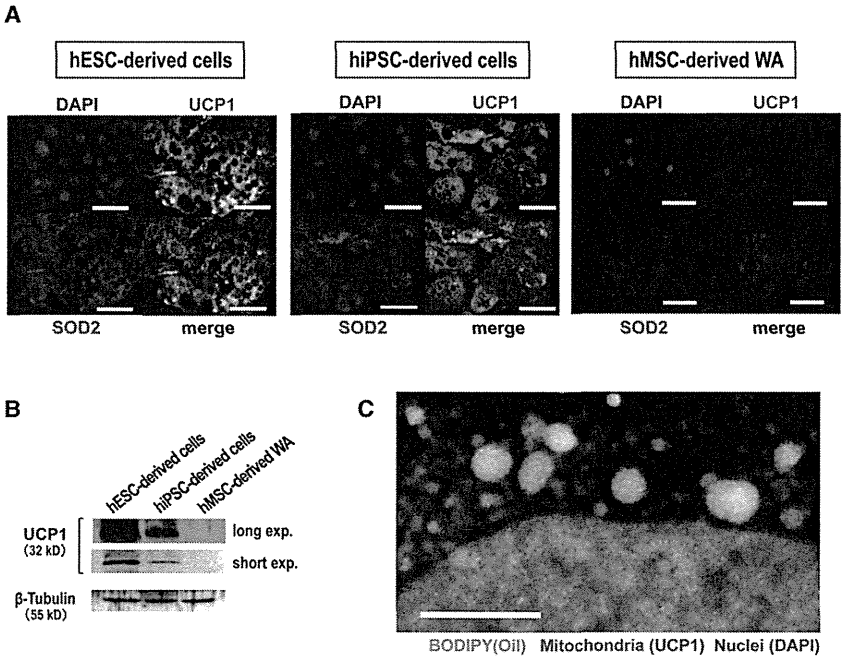

Figure 2. Analyses on Protein Expressions and Fine Structures

(A) Immunostaining using an anti-UCP1 and anti-SOD2 antibody as indicated. Scale bar, 50 μm.

(B) Western blotting using an anti-UCP1 as indicated.

(C) Lipid staining. hESC-derived differentiated cells were stained by an anti-UCP1 antibody (red) and BODIPY 493/503 (green). Scale bar, 5 μm.

(D) EM of hiPSC-derived cells (left) and hESC-derived cells (right). L, lipid droplets; M, mitochondria. Scale bar, 2 μm.

n = 3) (Figure 4D). Surprisingly, hMSCdWA-transplanted mice showed elevated homeostasis model assessment-insulin resistance (HOMA-IR) values compared not only with hESCdBA-transplanted mice ($p = 0.0003$; $n = 3$) but also with saline-injected mice ($p = 0.0011$; $n = 3$) (Figure 4E), indicating that hMSCdWA induces insulin resistance despite its favorable effect on lipid metabolism. Similar results were obtained when 6-week-old younger mice were used for the assay (data not shown). As shown in Figure 4F, oral glucose tolerance tests (OGTTs) further demonstrated that hESCdBA transplantation reduced 15 min blood glucose values compared to saline injected ($p = 0.010$; $n = 3$), while hMSCdWA-transplanted mice exhibited elevated 30 min blood glucose values compared not only with hESCdBA-transplanted mice ($p = 0.0034$; $n = 3$) but also with saline-injected mice ($p = 0.0055$; $n = 3$). Similar results were obtained when 6-week-old younger mice were used for the assay (data not shown), confirming that hMSCdWA transplantation deteriorates glucose metabolism. The different effects between hESCdBA and hMSCdWA were not due to the difference in cell survival, as we clearly detected the existence of transplanted cells (Figure S4A). Moreover, deterioration of glucose metabolism by hMSCdWA transplantation could not be attributed to inflammation, because we did not observe any signs of inflammation, such as macrophage infiltration (Figure S4B). In addition, hMSCdWA did not express tumor necrosis factor α (*TNFA*), and it expressed only a low level of *IL1B* (Figure S4C).

We also examined longer-term effects of hPSCdBA transplantation using immunocompromised NOG mice (Ito et al., 2002). Fasting blood glucose level-lowering effects of hESCdBA were determined at least for 3 weeks (Figure 4G). Cells with multilocular lipid droplet (Figure 4H) that expressed UCP1 (Figure 4I) and human HLA-A,B,C (Figure 4J) were determined by histological analyses. Around the graft tissue, microvasculatures were also detected (Figure 4H arrowheads).

Finally, we assessed possible therapeutic effect of hESCdBA on hMSCdWA-induced deterioration of glucose metabolism. Although no significant changes in fasting blood glucose values and HOMA-IR values were observed (Figure 4K and 4L), cotransplantation of an equivalent number of hESCdBA ameliorated the deleterious effect of hMSCdWA, significantly lowering the 30 min blood glucose values ($p = 0.0014$; $n = 3$) (Figure 4M).

All those findings together indicate that (1) hPSCdBAs improve both lipid and glucose metabolism, (2) hMSCdWA improved lipid but deteriorates glucose metabolism, and (3) hPSCdBAs ameliorate adverse effects of hMSCdWA on glucose metabolism.

(D) BA differentiation in the presence or absence of HC. Microscopy (upper) and expressions of *PRDM16* (lower left) and *UCP-1* (lower right) by real time PCR were shown. Scale bar, 50 μm. The error bars represent average ± SD ($n = 3$).

(E) Expression of BAT-selective, BAT/WAT-common, and WAT-selective genes examined by RT-PCR. I, immature hPSC; D, differentiated hPSC; WA, hMSCdWA.

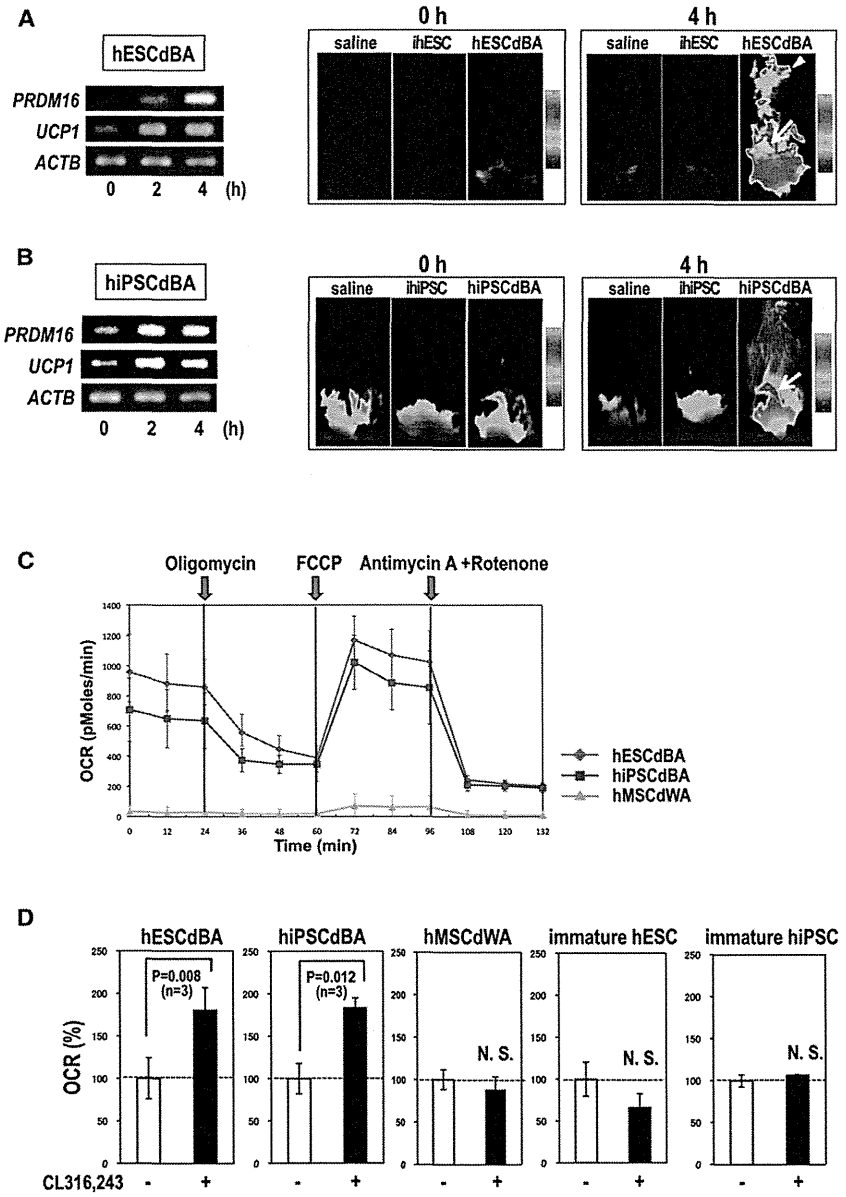

Figure 3. Thermogenic and Mitochondrial Respiratory Activation

(A and B) Thermogenesis studies. hESCdBA (A) and hiPSCdBA (B) were treated with isoproterenol. Gene expression was examined by RT-PCR over time (A, left; B, left). Thermographic images of mice transplanted with saline, immature hESC (ihESC), hESCdBA, immature hiPSC (ihiPSC), or hiPSCdBA before and after isoproterenol treatments are shown (A, right; B, right). Arrows indicate regions of transplantation; arrowheads indicate areas of endogenous murine BAT.

(C) Mito stress tests were performed using hESCdBA, hiPSCdBA, and hMSCdWA as indicated.

(D) OCR was measured in hESCdBA, hiPSCdBA, hMSCdWA, immature hESCs, and immature hiPSCs after a 4 hr incubation with or without CL316,243. The error bars in (C) and (D) represent average ± SD (n = 3).

Signaling for BA Differentiation

To confirm that our differentiation technique correctly reproduced classical BAT development via myoblastic differentiation (Timmons et al., 2007; Seale et al., 2008; Sun et al., 2011), the expression of a series of developmental markers was examined. As shown in Figure 5A, myoblastic *MYF5* expression was transiently upregulated during the initial floating culture step of differentiation. Moreover, the expression of a paraxial mesoderm marker, platelet-derived growth factor receptor α (*PDGFRA*) (Sakurai et al., 2006), was upregulated. By contrast, the levels of immature mesenchymal stem cell marker, *NG2* and *PDGFRB* (Crisan et al., 2008), as well as a lateral plate mesoderm marker, VEGFR2 (Sakurai et al., 2006), were reduced. The precedence of myoblastic differentiation was further confirmed by the transient induction of PAX3/7, which are involved in myogenic commitment (Figure 5B). Thus, our method correctly mimics the classical BAT development but not a brite adipocyte pathway via immature mesenchymal stem cell differentiation.

We further evaluated the detailed role of each hematopoietin. The absence of any one of the components of HC lowered the quality of BA differentiation, reducing cellular viability and/or percentages of multilocular lipid-containing cells (Figure 5C). Gene expression studies further showed that VEGF was required for *PRDM16* expression, whereas KITLG, IL6, or FLT3LG was required for subsequent *UCP1* expression (Figure 5D). Surprisingly, depletion of either KITLG, IL6, or FLT3LG paradoxically induced the expression of a WAT marker, phosphoserine aminotransferase 1 (*PSAT1*) (Seale et al., 2007), and a lateral plate mesoderm marker, vegfr2. Thus, the HC is essential for the differentiation of hPSCs into classical BA, and the omission of any of the HC components results in WAT lineage commitment.

We also examined intracellular signaling by performing inhibitor analyses. Because a BMPR1a inhibitor (BMPR1a-i) and p38 MAPK inhibitor (p38-i) reportedly hamper BA differentiation (Sellayah et al., 2011), effects of these two inhibitors, along with those of a MAP kinase-ERK kinase (MEK) inhibitor (MEK-i), were examined. We found that BMPR1a-i induced massive cell death during the floating culture step of BA differentiation (Figure 5E, second left). Cell death had been induced as early as day 1 (data not shown). Similar results were obtained from the case of AKT inhibitor (AKT-i). (Figure 5E, right). Thus, BMPR1a-dependent signaling is required for the survival of immature sphere-forming progenitor cells, from which mature BA will be produced. We then followed up the p38-i- and MEK-i-treated

cells until day 10, when mature BA was generated. In the case of hESC, p38-i treatment reduced the number of lipid droplet-containing cells (Figure 5F, upper middle), while MEK-i treatment exerted minimal effects (Figure 5F, upper right). Compatible to these morphological findings, p38-i treatment, but not MEK-i treatment, lowered *PRDM16* and *UCP1* expression levels (Figure 5G, left half). By contrast, p38-i treatment exerted minimal effects on hiPSCs (Figure 5F, lower middle), whereas MEK-i treatment induced cogeneration of the cells with unilocular lipid droplets (Figure 5F, lower right). Compatibly, *PRDM16* and *UCP1* expressions were only slightly reduced in p38-i-treated hiPSCs but clearly reduced in MEK-treated hiPSCs (Figure 5G, right half). Therefore, p38 MAPK and ERK signaling play important roles in BA differentiation depending on the lines or kinds of hPSCs.

A Functional Link between BA and Hematopoiesis

There has been a controversy regarding the effect of BM adipocytes on the proliferation and differentiation of committed HPCs. For example, murine BM adipocytic lines are reportedly capable of supporting lymphopoiesis (Gimble et al., 1990) and granulopoiesis (Gimble et al., 1992), whereas human BM-derived fat cells generated by a dexamethasone/insulin treatment reduce colony-forming capacities of HPCs (Ookura et al., 2007). We hypothesized that the controversy came from the heterogeneity of BM adipocytes and that BA, but not WA, serves as a stroma for committed HPCs for the following reasons: (1) hematopoietic stromal cells essential for maintaining CFU-S exhibit morphological resemblance to BA rather than to WA (Dexter et al., 1977); (2) the murine embryo-derived C3H10T1/2 cell line (Reznikoff et al., 1973), which differentiates into mature BAT on BMP7 treatment (Tseng et al., 2008), is widely used as a feeder for the hematopoietic differentiation of monkey (Hiroyama et al., 2006) and human (Takayama et al., 2008) ESCs; (3) BM is replaced by WA in severe myelosuppressive states including aplastic anemia; and (4) treatment with dexamethasone/insulin induces differentiation into WA but not BA.

To validate our hypothesis, human umbilical cord blood $CD34^+$ HPCs were cultured on hESCdBA layers for 1 week in the absence of any recombinant hematopoietic cytokines. Then, floating cells were subjected to intrabone marrow transplantation (IBM-T) into alymphocytic NOG mice, and after 8 weeks, splenic chimerisms were measured to assess the expansion of CFU-S. For a control, $CD34^+$ cells were directly transplanted without culturing on hPSCdBA layers (Figure 6A). As shown in Figure 6B, splenic chimerisms were significantly higher in hPSCdBA-cocultured $CD34^+$-transplanted mice than in mice with direct transplantation ($p = 0.041$; $n = 3$). Moreover, percentages of human CD33-positive myeloid cells were larger in cocultured $CD34^+$-transplanted mice (4.8 ± 0.13 versus 3.0 ± 0.19; $p = 0.00022$; $n = 3$, data not shown), while no significant changes in B lymphocyte percentages were observed (data not shown). These findings indicate that hPSCdBA serves as a stroma for MPCs, promoting their expansion/differentiation and homing to the spleen.

We also examined the expression of hematopoietic cytokines involved in the expansion and differentiation of committed HPCs. Various hematopoietin genes including thrombopoietin (*THPO*), *IL6*, *IL3*, colony-stimulating factor 3 (*CSF3*), colony-stimulating factor 2 (*CSF2*), and erythropoietin (*EPO*) were expressed in hESCdBA (Figure 6C, middle lanes) and hiPSCdWA (data not shown). On the other hand, hMSCdWAs expressed only *IL6* among these hemopoietins (Figure 6C, right lanes). Moreover, the expression levels of the hematopoietin genes in hESCdBA (Figure 6D) and hiPSCdBA (data not shown) were upregulated by isoproterenol treatments, further supporting the notion that hPSCdBA serves as stromal for committed HPCs.

To evaluate in vivo relevance, we examined whether isoproterenol treatment could enhance the recovery from antitumor agent-induced myelosuppression by enhancing the expansion/differentiation of MPCs. Mice were treated with 5-fluorouracile (5-FU), and bone marrow cells were collected and analyzed over time (Figure 6E). As reported by Hofer et al. (Hofer et al., 2007), 5-FU-treated mice were at the nadir at day 3, when a decline in total enucleated cell number (11.33 ± 1.74 versus 4.87 ± 0.96 [$\times 10^6$], $p = 0.0023$; $n = 3$) (Figure 6F) as well as a reduction in early myeloid cells (Figures S5A–S5C) were observed. Although total cell number (8.70 ± 0.40; $n = 3$) (Figure 6F) and the percentages of R1 fraction (Figures S5A and S5B) were eventually upregulated at day 7 as a sign of a recovery from myelosuppression, the mice still suffered from a shortage of mature myeloid cells (Figures S5A–S5C). By contrast, isoproterenol-treated mice showed higher enucleated cell number (10.93 ± 1.14, $p = 0.032$; $n = 3$) (Figure 6F) with significantly larger R2 fraction percentages (Figures S5A and S5B). Cytological studies confirmed all those findings (Figure S5C).

The existence of BA in BM has long been suggested despite the lack of direct evidence (reviewed in Motyl and Rosen, 2011). A relationship between osteoblast and BA was reported in mice (Calo et al., 2010). Moreover, murine BM fat reportedly expresses various BA-selective messages (Krings et al., 2012). To assess the possible existence of BA in human BM, expressions of BAT-specific markers, *UCP1* and *PRDM16*, were examined using commercially available human BM RNA samples. As shown in Figure 7A, expression of both genes was detected by RT-PCR, whereas they were undetectable in human BM-originated MSC-derived WA (hBM-MSCdWA). To further assess the existence of active BM-BAT in vivo, ^{18}F-FDG-PET/CT examinations were performed in healthy young volunteers (24.8 ± 5.8 of age; $n = 20$) with or without cold stimuli (Saito et al., 2009; Yoneshiro et al., 2011). We identified cold-stimulated ^{18}F-FDG uptake in vertebral BM (Figures 7B–7D), whose signal intensities showed an intimate correlation with those of BATs ($p < 0.001$), but not of those of brain, heart, spleen, or muscle (Figures S6A and S6B). The presence of vertebral BM was histologically examined using 3-week-old murine vertebral BM samples: we successfully detected the cells with BA morphologies (Figure 7E) that were positive for UCP1 protein expression (Figure 7F). Collectively, those findings strongly suggest the presence of functional BA in the BM of vertebrae.

DISCUSSION

We established a highly efficient method for the differentiation of hPSCs into functional BAs. This is the first success in generating functional classical BA pluripotent stem cells without exogenous gene transfer. By virtue of its technological merits, our method provides a valuable tool for BAT research. Functional

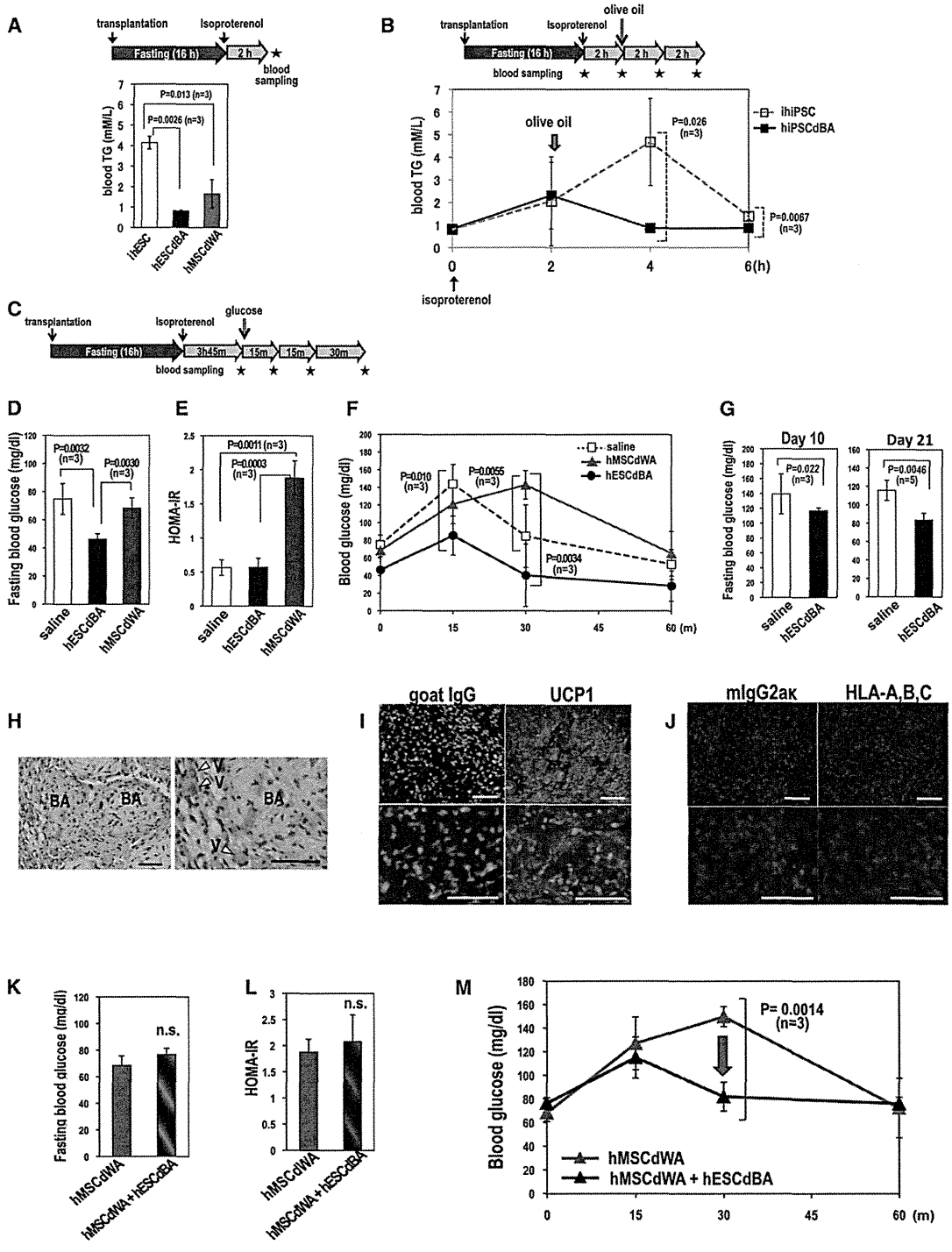

Figure 4. Metabolic Improvement by hPSC-Derived BA Transplantation

(A) Blood TG clearance tests. Immunocompetent ICR mice were transplanted with immature hESCs (ihESC) (n = 3 mice), hESCdBA (n = 3 mice), or hMSCdWA (n = 3 mice). After 16 hr starvation, isoproterenol was administrated and blood TG levels were measured.

(B) Oral fat tolerance tests. ICR mice were transplanted with immature hiPSC (ihiPSC) (n = 3 mice) or hiPSCdBA (n = 3 mice). Olive oil was orally loaded, and blood TG levels were measured over time after isoproterenol treatments.

(C–F) OGTT. ICR mice were injected with saline (n = 3 mice), hESCdBA (n = 3 mice), or hMSCdWA (n = 3 mice), and OGTT was performed (C). Fasting blood glucose levels (D), HOMA-IR (E), and blood glucose values after oral glucose loading (F) are shown.

(G–J) Immunocompromized NOG mice were injected with saline or transplanted with hESCdBA. At indicated time points, fasting blood glucose levels were measured. Three mice (day 10) or five mice (Day 21) were used for each condition (G). Histological studies were performed by HE staining (H) and